Journal for ImmunoTherapy of Cancer

Generation of cDC-like cells from human induced pluripotent stem cells via Notch signaling

Kenichi Makino,[1,2] Mark D Long,[3] Ryutaro Kajihara,[1] Satoko Matsueda,[1] Takaaki Oba,[1,4] Kazunori Kanehira,[5] Song Liu,[3] Fumito Ito [1,6,7,8]

To cite: Makino K, Long MD, Kajihara R, *et al*. Generation of cDC-like cells from human induced pluripotent stem cells via Notch signaling. *Journal for ImmunoTherapy of Cancer* 2022;**10**:e003827. doi:10.1136/jitc-2021-003827

► Additional supplemental material is published online only. To view, please visit the journal online (http://dx.doi.org/10.1136/jitc-2021-003827).

KM, MDL and RK contributed equally.

Accepted 19 December 2021

For numbered affiliations see end of article.

Correspondence to
Dr Fumito Ito;
fumito.ito@med.usc.edu

ABSTRACT

Background Dendritic cells (DCs) play critical roles in regulating the innate and adaptive immune responses, and have long been a major focus of cancer immunotherapy. Accumulating evidence suggests that conventional type 1 DCs (cDC1s) excel in cross-presentation of exogenous antigens on MHC-I molecules and induction of antitumor CD8$^+$ T cell immunity; however, obtaining large numbers of cDC1s is difficult. The use of reprogramming and differentiation technology is advantageous for obtaining unlimited numbers of autologous cDC1s especially for therapeutic interventions where repeated vaccinations are required. However, generation of cDC1s from human induced pluripotent stem cells (iPSCs) remains elusive.

Methods Human iPSCs established from peripheral blood T cells and monocytes were differentiated to myeloid cells under on-feeder or feeder-free culture conditions in vitro. Phenotype, genomic and transcriptomic signature, and function of human iPSC-derived DCs were analyzed. The role of Notch signaling for the generation of HLA-DR$^+$ cells from human iPSCs was interrogated by a loss- and gain-of-function approach.

Results Flow cytometric analyses and single-cell profiling of HLA-DR$^+$ cells revealed that human iPSCs gave rise to CD141$^+$XCR1$^+$CLEC9A$^+$ cells (cDC1s), CLEC4A^{hi}CLEC10A$^-$CD1c$^+$ cells (cDC2As), CLEC4A^{lo}CLEC10A$^+$CD1c$^+$ cells (cDC2Bs), CD163$^-$CD5$^+$CD1c$^+$ cells (CD5$^+$cDC2s), and AXL$^+$SIGLEC6$^+$ cells (AS-DCs) on OP9 feeder cells expressing the Notch ligand delta-like 1 (OP9-DL1) while the majority of iPSC-derived cells differentiated on OP9 cells were CD163$^+$CD5$^-$CD1c$^+$ cells (DC3s) and monocytes. Plasmacytoid DCs were not differentiated from iPSCs on either OP9 or OP9-DL1 cells. Inhibition of Notch signaling during co-culture of iPSC-derived CD34$^+$ hematopoietic progenitor cells with OP9-DL1 cells abrogated generation of cDC1s, cDC2As, cDC2Bs, CD5$^+$cDC2s, and AS-DCs but increased frequency of DC3s. Notch-activated human iPSC-derived XCR1$^+$CLEC9A$^+$HLA-DR$^+$CD11c$^+$ cells exhibited similar gene expression profile with peripheral blood cDC1s. Human iPSC-derived DCs have phagocytic, T-cell proliferative, and cytokine-producing functions.

Conclusions Our study demonstrates a critical role of Notch signaling in regulating developmental pathway of human cDCs. These findings provide insights into the future development of personalized treatment with unlimited numbers of autologous cDCs from human iPSCs.

INTRODUCTION

Dendritic cells (DCs) are a diverse population of specialized antigen-presenting cells that link innate and adaptive immunity, and crucial in the induction of immune responses to pathogens and tumors as well as for the maintenance of self-tolerance.[1] DC-based immunotherapy has been tested for harnessing the potential of a patient's own immune system; however, which subsets of DCs can be used to design efficient vaccines remains to be determined.[2] Although numerous clinical studies using monocyte-derived DC have showed DC vaccination has low toxicity and induces tumor-specific immune responses, the number of objective clinical responses is limited.[2–4] Compelling evidence indicates that naturally occurring (primary) DC subsets are phenotypically and transcriptionally distinct from ex vivo–generated monocyte-derived DCs.[3–11]

Of the different naturally occurring DCs, the Batf3-dependent conventional type 1 DC (cDC1) subset represents a promising alternative to monocyte-derived DCs for vaccination purposes. There is a growing body of evidence that cDC1s have the superior capacity to cross-present exogenous antigen to CD8$^+$ T cells, produce IL-12 in response to innate and T cell–derived stimuli, induce Th1-type T cell responses, and play a critical role in antitumor T-cell responses.[12–15] However, cDC1s are rare (<0.2%–0.3%) in peripheral blood mononuclear cells (PBMCs), and isolating a sufficient number of cDC1s for repeated therapeutic vaccination is difficult.[3 5 6]

This limitation can be theoretically overcome by using induced pluripotent stem cells (iPSCs) as an unlimited source of autologous cDC1s. Previous studies reported successful generation of DCs from human iPSCs in co-culture with feeder cells in the presence of interleukin (IL)−4 and GM-CSF.[16 17] However, requirements for the generation of cDC1s

from human iPSCs remains to be clarified. Although previous studies showed differentiation of human iPSCs into CD141$^+$ DCs without Notch signaling,[18 19] emergent evidence revealed a key role of Notch signaling in differentiation of mouse and human hematopoietic CD34$^+$ progenitors into cDC1s.[20 21]

Here, we report efficient generation of functional cDC1-like cells from human iPSCs. Mechanistic studies illustrate non-redundant requirement of Notch signaling in differentiation of cDC1-like cells from human iPSCs. High-throughput characterization of human iPSC-derived HLA-DR$^+$ cells not only shows the presence of DCs with cDC1 signatures resembling peripheral blood cDC1s but also reveals the heterogeneity of CD1c$^+$ DCs derived from human iPSCs.

METHODS

Human samples

After written informed consent, a venous blood sample of up to 30 mL was collected in EDTA tubes (BD Biosciences) from a healthy donor. PBMCs were isolated using Lymphocyte Separation Medium (Corning) density gradient centrifugation.

Mice

NOD/SCID/IL-2Rγ-deficient (NSG) mice were purchased from the Jackson Laboratories. Mice were 7 to 10 weeks old at the beginning of each experiment, and maintained under specific pathogen-free conditions and housed in the Laboratory Animal Resources facility. All animal studies were conducted in accordance with and approved by the Institutional Animal Care and Use Committee (IACUC) at the Roswell Park Comprehensive Cancer Center.

Cell lines

OP9 mouse bone marrow stromal cells and OP9 cells expressing the Notch ligand Delta-like-1 (OP9-DL1) were purchased from RIKEN (Japan). MS5-DL1 cells were purchased from MilliporeSigma. OP9-DL1 and MS5-DL1 cells express green fluorescent protein (GFP). OP9, OP9-DL1, and MS5-DL1 cells were cultured on gelatin-coated dishes in OP9 medium: αMEM supplemented with 25% non-heat inactivated fetal bovine serum (FBS; Biowest), 0.5% penicillin/streptomycin, and 2.2 g/L of sodium bicarbonate (MilliporeSigma). SNL cells (Cell Biolabs, Inc.) were cultured in DMEM containing 7% FBS (MilliporeSigma), 2 mM L-glutamine, and 0.5% penicillin/streptomycin. Human embryonic stem cells (ESCs) (H9; WiCell) were maintained on mitomycin C–inactivated SNL feeder cells in human ESC media which consisted of Primate ESC Medium (Reprocell) and 4 ng/mL basic fibroblast growth factor (bFGF; ThermoFisher Scientific), and used as controls for characterizing the pluripotency and differentiation capacity of generated iPSCs. These cell lines were authenticated by morphology, phenotype and growth, and routinely screened for *Mycoplasma*, and were maintained at 37°C in a humidified 5% CO_2 atmosphere.

Establishment of iPSCs from peripheral blood T cells

Peripheral blood T cells were reprogrammed to human iPSCs as described.[22–24] In brief, T cells were activated with plate-bound anti-CD3 Ab (10 µg/mL) (BD Biosciences #555336) and soluble anti-CD28 Ab (5 µg/mL) (BD Biosciences #555725) in X-VIVO 15 medium (Lonza) containing 5% FBS, 1 M HEPES (Gibco), 2 mM L-glutamine (Gibco), and penicillin/streptomycin (Gibco) and recombinant human IL-2 (60 IU/mL; Prometheus Laboratories Inc.) in a 24-well plate at 1×10^6 cells/well for 5 days. On day 5, T cells were reactivated with plate-bound anti-CD3 Ab and soluble anti-CD28 Ab and IL-2 (60 IU/mL) in a 24-well plate at 1×10^5 cells/well for 24 hours. On day 6, T cells were infected with Sendai virus (SeV) vectors that individually carried each of OCT3/4, SOX2, KLF4, and c-MYC (CytoTune-iPS 2.0 Reprogramming Kit; ThermoFisher Scientific) at 20 multiplicity of infection (MOI). After 24 hours of infection, the cells were collected and transferred to a 10 cm dish that contained mitomycin C–inactivated SNL feeder cells in human ESC media. The ESC medium was changed every other day until the colonies were picked. Then, the ESC culture medium was changed every day and the cells were passaged using 1 mg/mL collagenase Type IV (Invitrogen) every 5–6 days.

Establishment and maintenance of iPSCs from peripheral blood monocytes

Peripheral blood monocytes were reprogrammed to human iPSCs as described.[25 26] Briefly, the isolated PBMCs were incubated for 7 days in StemFit (AJINOMOTO, Tokyo, Japan) media containing cytokines, human IL-3 (20 ng/mL; Peprotech), IL-6 (50 ng/mL; Peprotech), thrombopoietin (TPO; 10 ng/mL; Peprotech), stem cell factor (SCF; 50 ng/mL; Peprotech), granulocyte colony-stimulating factor (G-CSF; 10 ng/mL; Peprotech, and FMS-like tyrosine kinase 3 ligand (Flt3L; 20 ng/mL; R&D Systems). The incubated monocytes were reprogrammed to iPSCs by transduction of reprogramming factors by SeV using CytoTune-iPS 2.0 Reprogramming Kit at 20 MOI. The reprogrammed cells were cultured on iMatrix-511 or iMatrix-511 silk (Nippi, Tokyo, Japan) coated plate and their medium was replaced with StemFit iPSC medium containing bFGF. The established iPSCs were cloned and their pluripotency characterized by expression of markers and teratoma formation in immunodeficient mice.

Gene expression analysis by RT-PCR

Total RNA samples were isolated with TRIzol reagent (Life Technologies) and purified, according to the manufacturer's instructions. One microgram total RNA was used for cDNA synthesis by RT-PCR with SuperScript III Reverse Transcriptase (Life Technologies) and random primer, according to the manufacturer's instructions. cDNA was amplified by PCR with Platinum Taq DNA Polymerase

(Life Technologies) and various sets of primers showed in online supplemental table S1.

Immunocytochemistry

Human iPSCs were cultured on iMatrix-511 coated plate and incubated for 5 to 7 days. After formation of iPSC colonies, they were fixed with 4% paraformaldehyde. Immunofluorescence staining was performed using the following primary antibodies: anti-OCT3/4 antibody (Santa Cruz Biotechnology); anti-SSEA4 antibody (MilliporeSigma). Alexa Fluor 488–conjugated anti-mouse IgG antibody (Jackson ImmunoResearch) was used for the secondary antibody.

Generation of DCs from human iPSCs on feeder cells

To generate hematopoietic progenitor cells (HPCs), iPSCs were co-cultured with OP9 cells as described.[17] In brief, human iPSCs (2×10^4/well) were cultured in a 6-well plate for 7 days before differentiation. Human iPSCs from two wells of the 6-well plate were gently detached by a cell scraper, and placed on a gelatin pre-coated OP9 overconfluent 10 cm dish in 10 mL of αMEM containing 10% FBS and monothioglycerol (100 µM; MilliporeSigma) (day 0). Medium was replaced by 20 mL of fresh medium on day 1, and half of the volume of them was replaced on days 4, 6, 8, and 11. On day 13, colonies were treated for 30 min with 5 mL of collagenase Type IV (50 U/mL) and subsequently dissociated for 30 min at 37°C using 5 mL of 0.05% Trypsin-EDTA (Gibco). To remove stromal cells, dissociated cells were resuspended adding 5 times OP9 medium plated on plastic at 37°C for 45 min and floating cells were collected. To further remove stromal cells and aggregated cells, cells were passed through a 70 µm filter. $CD34^+$ cells were isolated from the generated cell population by MACS (Magnetic activated cell sorting; Miltenyi Biotec), and placed on gelatin pre-coated OP9 or OP9-DL1 cells in 10 mL of αMEM containing 10% FBS with GM-CSF (20 ng/mL; Peprotech), Flt3L (100 ng/mL), and SCF (20 ng/mL) for 2 weeks. Medium was replaced once a week. In some experiments, we added a γ-secretase inhibitor, N-[N-(3,5-difluorophenacetyl)- L-alanyl]-S-phenylglycine t-butyl ester (DAPT; 5 µM; MilliporeSigma #565790) or DMSO when we co-culture human iPSC-derived $CD34^+$ cells with OP9-DL-1 cells.

Generation of DCs from human iPSCs on feeder-free condition

We added Flt3L to the previously described protocol[19] for generation of $CD141^+XCR1^+CLEC9A^+HLA\text{-}DR^+$ cells under feeder-free condition. In brief, we cultured human iPSCs in 4 mL/well of XVIVO-15 in a 6-well plate supplemented with 1 mM sodium pyruvate (Gibco), 0.1 mM non-essential amino acid (NEAA, Gibco), 2 mM L-glutamine, and 0.05 mM 2-mercaptoethanol (Gibco) in the presence of the cytokine cocktail containing Flt3L (1 µg/mL), GM-CSF (50 ng/mL), SCF (20 ng/mL), vascular endothelial growth factor (VEGF, 50 ng/mL; Peprotech), and bone morphogenetic protein 4 (BMP4; 50 ng/mL; Peprotech). Half of the medium was replaced every 2 days from day 2 of culture. BMP4 was removed from day 5 onward, followed by VEGF (day 14) and SCF (day 19). On days 14–28 of culture, IL-4 (Peprotech) was added to the medium at 10 ng/mL (days 14, 15), 20 ng/mL (days 16, 17), 40 ng/mL (days 18, 19), 60 ng/mL (days 20, 21), 80 ng/mL (days 22, 23), and 100 ng/mL (days 24–28). DCs were harvested on day 28 using gentle pipetting.

Teratoma formation and histological analysis

Undifferentiated human iPS cells (1×10^6) suspended in 100 µL of DMEM containing 10% FBS were injected into the subcutaneous tissue of NSG mice. Four weeks after injection, tumors were surgically dissected from the mice. Samples were fixed in PBS containing 10% paraformaldehyde and embedded in paraffin. Paraffin-embedded samples were stained with H&E for histological analysis.

Cytology

Human iPSC-derived differentiated cells were harvested and Hema 3 leukocyte staining were performed. Briefly, 5×10 cells in 100 µL PBS were centrifuged on microscope slides using a Shandon Cytospin 2 Cytocentrifuge (Thermo Electron). The cytocentrifuged cell smears were fixed and stained with Hema 3 stain kit (Fisher Scientific).

Microscopy

Images of Hema 3–stained cytospins and H&E-stained teratoma were taken on an Olympus BX45TF inverted microscope with an Olympus DP27 digital camera.

Flow cytometry

Phenotypic analysis of PBMCs and human iPSC-derived cells was performed as described.[22 24 27] Briefly, single cell suspensions of PBMCs and human iPSC-derived cells were stained with a master mix of antibodies (Abs) for surface stains after Fc block (human Fc block; BD Biosciences) for 20 min at room temperature. Antibodies used in this study are listed in online supplemental table S2. Live/Dead Fixable Aqua Dead Cell Stain Kit (ThermoFisher Scientific) and LIVE/DEAD Fixable Near-IR Dead Cell Stain kit (ThermoFisher Scientific) were used to exclude dead cells from the analysis. Samples were analyzed using LSRII or LSRFortessa (BD Biosciences) with FlowJo software (TreeStar).

Functional characterization of generated human iPSC-DCs

Cell surface phenotype was analyzed by flow cytometer. Phagocytosis was evaluated using the pHrodo Green Zymosan Bioparticles (ThermoFisher Scientific), as described.[18] In proliferation assay, peripheral blood T cells were isolated by immunomagnetic negative selection from the same blood donor of iPSCs using EasySep Human T cell Isolation Kit (STEMCELL Technologies). T cells were labeled by Carboxyfluorescein Succinimidyl Ester (CellTrace CFSE Cell Proliferation Kit; ThermoFisher Scientific) and cultured with $HLA\text{-}DR^+$ iPSC-DCs at 37°C with 5% CO_2 in presence of positive control peptide pool of major histocompatibility complex (MHC) class I-restricted and II-restricted epitopes (CEFX-3 and CEFX-4;

JPT Peptide Technologies) and IL-2 (60 IU/mL). In some experiments, we magnetically sorted CLEC9A$^+$ cells by staining with PE anti-human CLEC9A followed by anti-PE MicroBeads (Miltenyi Biotec) before co-culture with CFSE-labeled T cells. The DC:T cell ratio was 1:5. At day 5, cells were harvested and analyzed by flow cytometer. To identify cytokine production from human iPSC-derived DCs, cells were stimulated with an activation cocktail consisting of polyinosinic:polycytidylic acid (poly(I:C), 25 µg/mL; InvivoGen #tlrl-pic), R848 (2.5 µg/mL; InvivoGen #tlrl-r848), CpG oligodeoxynucleotides (ODN) 2216 (1 µM; InvivoGen #tlrl-2216), and lipopolysaccharide (LPS, 100 ng/mL; MilliporeSigma #L6529) for 6 hours at 37°C, 5% CO_2. BD GolgiPlug (BD Biosciences) was added to the culture in last 4 hours.

Single cell RNA sequencing (scRNAseq)

Sample preparation

For the scRNAseq experiments, single cell suspensions of human iPSC-derived DCs were stained with a master mix of antibodies for surface staining including Live/Dead Fixable Aqua Dead, CD11c, and HLA-DR after Fc block. Sorting of live HLA-DR$^+$ cells were performed on a BD FACSAria II (BD Biosciences).

Single-cell RNA sequencing library generation

Droplet-based 3′ end massively parallel scRNAseq was performed by encapsulating flow-cytometry-sorted cells into droplets and libraries were prepared using Chromium Single Cell 3′ Reagent Kit V3 according to manufacturer's protocol (10x Genomics). To minimize batch effect, library preparation was performed on all captured cells simultaneously, and all libraries were sequenced on a single Novaseq S1 flow cell on an Illumina Novaseq 6000 instrument.

Raw data processing, quality control for cell inclusion, and scRNAseq analysis

Raw sequence data demultiplexing, barcode processing, alignment (mm10), and filtering for true cells were performed using the Cell Ranger Single-Cell Software Suite (V.5.0.0), yielding cells (OP9: 5753 cells, and OP9-DL1: 4158 cells) with a mean of 29,643 reads/cell (97.60% mapping rate), median of 3172 genes/cell, 20,142 total unique detectable genes, and 11,353 median UMI counts/cell (online supplemental table S3). Subsequent filtering and downstream analyses were performed using Seurat (v3).[28] Genes expressed in less than 3 cells and cells that express less than 350 genes were excluded from further analyses. Additional filtering of cells was determined based on the overall distributions of total RNA counts (<55,000) and the proportion of mitochondrial genes (<12%) detected to eliminate potential doublets and dying cells, respectively. Additional detection of doublets was performed using Scrublet.[29] Thresholding for doublet detection was set based on total distribution of doublet scores (doublet threshold=0.2). Quantification of mitochondrial and ribosomal gene expression was calculated using the PercentageFeatureSet function, using gene sets compiled from the Mouse Genome Informatics database. Cell cycle phase scoring was accomplished against normalized expression via the CellCycleScoring function using mouse genes orthologous to known cell cycle phase marker genes.[30] Ultimately, we removed 982 cells (9.91% of total cells) after quality control assessment and included 8929 cells (OP9: 5283 cells and OP9-DL1: 3646 cells) for analysis. Normalization and variance stabilization were conducted using regularized negative binomial regression (sctransform) and sample data subsequently harmonized using anchor-based integration implemented with Seurat v3. Principle component analysis (PCA) was performed on integrated data and optimal dimensionality of the dataset was decided by examination of the Elbow plot as the total number of PCs where gain in cumulative variation explained was greater than 0.1% (PCs=40). The FindNeighbors function was used that implements a graph-based nearest neighbor clustering approach, and then the FindClusters function was used to identify final cell clusters (n=13) using a resolution of 0.08. Uniform manifold approximation and projection (UMAP) was applied for non-linear dimensional reduction to obtain a low dimensional representation of cellular states. Differential expression between clusters was determined using the MAST method via the FindMarkers function, using a minimum expression proportion of 25% and a minimum log fold change of 0.25. Unbiased cell type annotation was performed using SingleR.[31] Briefly, this framework allows for the annotation of scRNAseq data to reference transcriptome data sets of known origin to infer the cellular state of each input cell. The built in Novershtern Hematopoietic reference[32] was used for SingleR-based cell annotation. Mean expression of markers found within each cluster or cell annotation were used for subsequent analyses including heatmap visualization and pathway analysis. Reference-based mapping of hiPSC-DC–derived scRNA-seq data was performed against previously published datasets characterizing DC heterogeneity in human PB and spleen.[33–36] Raw counts were obtained from the Gene Expression Omnibus (GSE137710, GSE94820, GSE151087, GSE132566) and re-processed using a Seurat-based pipeline described previously. Cell annotations were obtained as reported in initial publication (GSE137710, GSE94820) or inferred from custom analysis using manuscript specific gene markers (GSE132566, GSE151087). Gene sets for single-cell enrichment analyses were pulled directly from reported cell type gene markers from each respective study. Reference-based mapping and label transfer of previously annotated cells was performed using the FindTransferAnchors and MapQuery functions implemented within Seurat. Reference-based mapping of hiPSC-DC–derived scRNA-seq data to the Azimuth PBMC global reference was performed using Azimuth (https://azimuth.hubmapconsortium.org/).

Pathway analysis

Gene set enrichment analysis (GSEA) of select differential expression profiles identified between groups or clusters was done using enrichR and clusterProfiler in R. Single-cell functional enrichment analysis was done using AUCell,[37] which applies an area under the curve method to query cell-to-cell pathway activity which is robust to noise typical of scRNAseq datasets. Six pathway databases (Hallmark, KEGG, Reactome, PID, BioCarta, and GO-BP) were compiled from the Molecular Signatures Database (MSigDB)[38] and used as a reference sets for functional enrichments. For GSEA, only gene sets with fdr adjusted p<0.05 were considered as significantly enriched. To visualize select functional enrichments, we generated heatmaps and/or lollipop plots of normalized enrichment scores (NES) of relevant biological pathways.

RNA Sequencing

The generated iPSC-derived DCs and PBMCs were stained with a master mix of antibodies for surface staining including Live/Dead Fixable Aqua Dead, XCR1, CLEC9A, CD11c, and HLA-DR after Fc block with human IgG. $CD11c^+HLA\text{-}DR^+CLEC9A^+XCR1^+$ cells were sorted on BD FACSAria II. Total RNA was prepared from these sorted DCs using the miRNeasy mini kit (Qiagen). TruSeq Stranded messenger RNA (mRNA) (Illumina) was used for library preparation. Quality control for raw reads was performed with fastqc. Transcript abundances were quantified from sequencing reads against the human reference genome (GRCh37.67) using salmon-0.14.1.[39] Raw feature counts were normalized and differential expression analysis carried out using DESeq2.[40] Differential expression rank order was used for subsequent GSEA, performed using the clusterProfiler package in R. Gene sets queried included the Hallmark, Canonical pathways, and GO Biological Processes Ontology collections available through the Molecular Signatures Database (MSigDB).[38]

RESULTS

Notch signaling facilitates generation of $CD141^+CLEC9A^+XCR1^+$ DCs from human iPSCs

Recent work revealed Notch-dependent differentiation of $Lin^-CD34^+CD43^+CD45^+$ myeloid progenitors into cDC1s,[20 21] while previous studies showed differentiation of human iPSCs into $CD141^+$ DCs without Notch signaling.[18 19] Therefore, it remains unclear whether Notch signaling is required for the generation of cDC1s from human iPSCs. To this end, we first sought to establish iPSCs from peripheral blood T cells using the SeV vector reprogramming system which has been shown to efficiently reprogram human and murine T cells.[23 41] Peripheral blood T cells were transduced with reprogramming factors via SeV vectors 24 hours after activation with anti-CD3 and anti-CD28 Ab.[22–24] Twenty-four hours after gene introduction, the cells were replated onto feeder layers of SNL cells with ESC medium containing bFGF. To compare the differentiation capacity of human iPSCs of different origin and established by different methods, we also generated iPSCs from peripheral blood monocytes. PBMCs from the same donor were cultured with mononuclear cell medium containing IL-6, SCF, TPO, Flt3L, IL-3, and G-CSF for 7 days to enrich monocytes.[25 26] Peripheral blood monocytes were transduced by the SeV reprogramming system and, 24 hours later, transferred onto laminin-coated plate in StemFit medium containing bFGF. The established iPSCs derived from T cells (TiPSCs) and monocytes (MiPSCs) had morphology typical of human ESCs (online supplemental figure 1A). RT-PCR analyses showed that iPSCs expressed transcripts for the ESC marker *NANOG*, whereas they have lost SeV transcripts early on after a few passages (online supplemental figure 1B). Immunostaining revealed that iPSCs expressed the OCT3/4 and SSEA4 proteins (online supplemental figure 1C). On subcutaneous injection into NSG mice, human iPSCs gave rise to teratomas representing all three embryonic germ layers (online supplemental figure 1D).

For hematopoietic differentiation of human iPSCs, we used the bone marrow stromal cell line, OP9, as a feeder as previously described.[17] We cultured human iPSCs on OP9 cells for 13 days and observed mesodermal colonies (online supplemental figure 2A). To analyze phenotype of differentiated cells, cells were gated on the pan-human marker CD147 to gate out the fluorescent signal from remaining murine OP9 cells (online supplemental figure 2B). We found the majority of human ESC-derived and iPSC-derived $CD34^+$ cells expressed CD43 and/or CD45 (online supplemental figure 2C). To determine the role of Notch signaling in generation of cDC1s, we isolated $CD34^+$ cells from day 13 of co-culture and cultured them on OP9 or OP9-DL1 cells in the presence of SCF, GM-CSF, and Flt3L for 14 days (figure 1A). Approximately 1×10^6 cells were differentiated from $0.5\sim2\times10^5$ iPSCs on OP9 or OP9-DL1 cells. The analysis of cell morphology via cytospins revealed that differentiated cells were found to be myelomonocytic cells; mixture of granulocytic and monocytic cells was identified on OP9 feeder cells while myeloid cells with dendritic projections and veils typical of cells of dendritic lineage found on OP9-DL1 feeder cells (figure 1B).

We next aimed to define TiPSC-derived cells by conventional flow cytometry (online supplemental figure 3A). We found that co-culture with OP9-DL1 cells yielded substantially more $HLA\text{-}DR^+$ cells compared with control OP9 cells which had more monocytic cells expressing CD14, CD16, and/or CD163 (figure 1C). The majority of $HLA\text{-}DR^+$ cells differentiated on OP9 cells were $CD1c^+CD141^-$ DCs. In contrast, DL1-Notch signaling markedly increased the frequency of $CD141^+CLEC9A^+XCR1^+$ DCs (figure 1D). These cells also expressed CD1c consistent with previous studies showing CD1c expression in $CD141^+$ cDC1s differentiated from human $CD34^+$ cord blood progenitors in vitro and in Flt3L-induced $CD141^+$ cDC1s in vivo.[20 42 43] We found higher frequency of $HLA\text{-}DR^+$ cells expressing CD80, CD40, and CCR7 in coculture with OP9-DL1

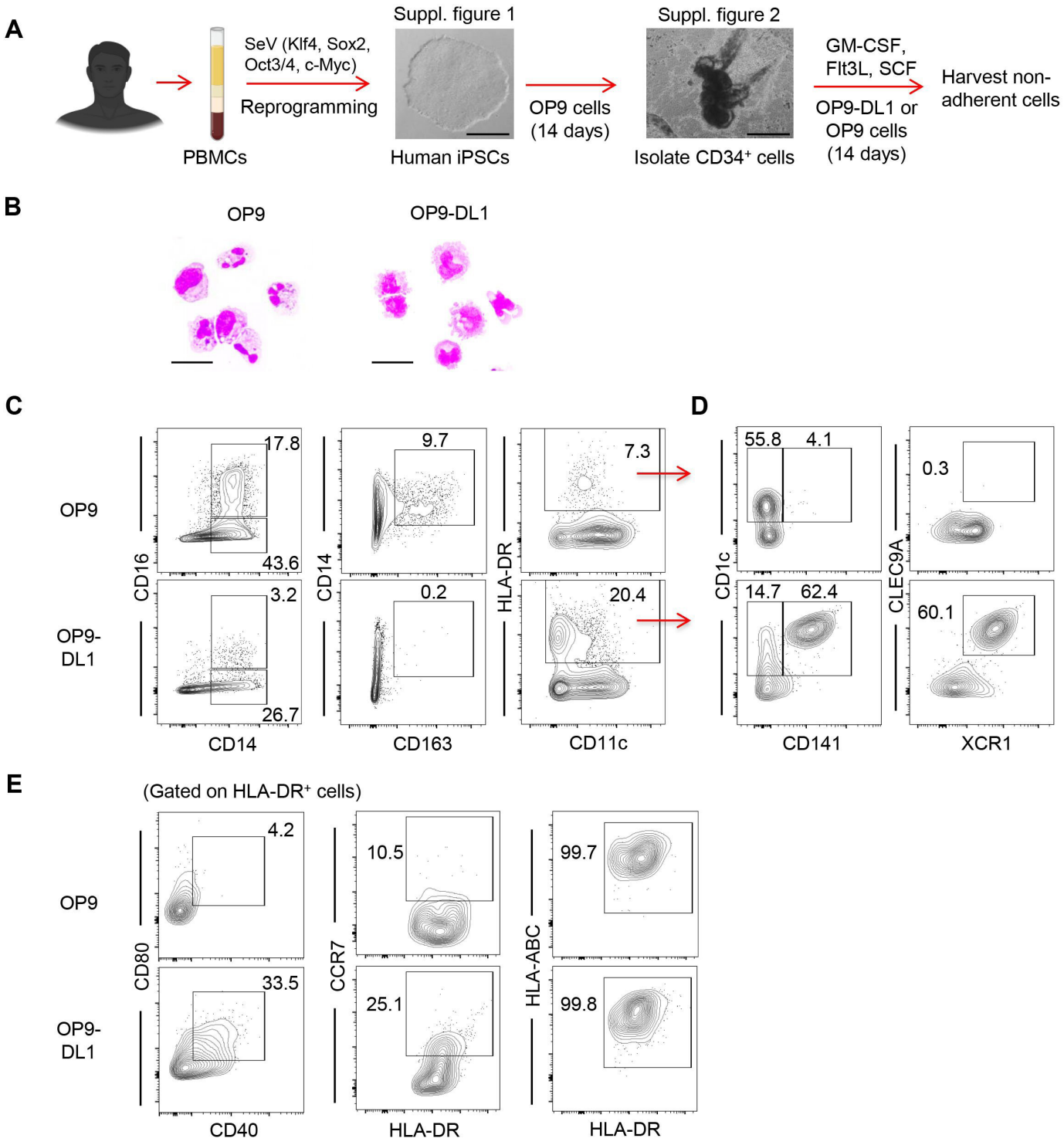

Figure 1 Notch signaling facilitates generation of CD141$^+$CLEC9A$^+$XCR1$^+$ DCs from human iPSCs. (A) Schematic illustration showing the generation of DCs from iPSCs (scale bar, 500 µm). (B) Hema 3-stained cytospins of human iPSC-derived cells on OP9 (left) and OP9-DL1 (right) feeder cells (scale bar, 10 µm). (C–E) Representative flow cytometric plots showing marker expression of human iPSC-derived cells on OP9 (upper) and OP9-DL1 (lower) feeder cells. Number denotes percent positive cells for each marker. Data shown are representative of three independent experiments.

compared with OP9 cells although there was no difference in HLA-ABC expression (figure 1E). Human ESCs and another TiPSC-derived clone (#2) similarly differentiated to cDC1-like cells on OP9-DL1 but not on OP9 cells (online supplemental figure 3B,C). We also examined whether TiPSCs could differentiate to cDC1-like cells on different feeder cells, MS5 expressing Notch ligand DL1 (MS5-hDLL1), and found that Notch signaling facilitated generation of CD141$^+$CLEC9A$^+$XCR1$^+$ DCs regardless of the type of feeder cells (online supplemental figure 3D). Furthermore, we addressed whether there was phenotypical difference between TiPSCs and MiPSCs differentiated

on OP9-DL1 cells. MiPSCs also gave rise to cDC1-like cells expressing CD141$^+$ and CLEC9A$^+$ (online supplemental figure 4A). We found both TiPSC-derived and MiPSC-derived HLA-DR$^+$ cells contained comparable frequency of CD80$^+$, CD40$^+$, and TLR3$^+$ cells (online supplemental figure 4B). Hereafter, TiPSC-derived DCs were used for further analyses.

Identification of various human iPSC-derived cDC subsets by single-cell RNA sequencing

Next, we carried out single-cell RNA-sequencing (scRNAseq) to further characterize iPSC-derived HLA-DR$^+$ cells. The corresponding fluorescence-activated cell sorting (FACS)–purified single live CD147$^+$GFP$^-$HLA-DR$^+$ cell populations differentiated on OP9 and OP9-DL1 cells were subjected to scRNAseq by using the 10x Genomics pipeline. This yielded data for 8929 high-quality cells after stringent filtering (OP9: 5283 cells; OP9-DL1: 3646 cells) (online supplemental figure 5A,B). Unsupervised clustering analysis identified 12 myelomonocytic clusters (cluster (C)0–10, 12) and a small cluster of erythroids (C11) (figure 2A–C and online supplemental figure 6). Human iPSCs differentiated on OP9-DL1 contained markedly increased frequency of DCs (C3, 5, 6, and 8) characterized by high levels of MHC class II–related genes (*HLA-DQB1*, *HLA-DQA1*, *HLA-DRB1*, *HLA-DRB5*, *HLA-DPA1*, and *HLA-DPB1*) (figure 2B–D and online supplemental figure 7). In contrast, a majority of OP9-differentiated iPSC-derived cells were computationally identified as monocytes (C0-2, 7, 9, 10, 12) and colony forming unit-monocytes (CFU-M: C4) (figure 2A–E and online supplemental table S4). Within the clusters expressing higher levels of MHC class II genes, C6 expressed genes and transcriptomes specific to cDC1s[11 20] such as *DNASE1L3*, *CADM1*, *SLAMF8*, *SNX22*, *GCSAM*, *CLNK*, *CLEC9A*, *BATF3*, and *XCR1*, and antigen processing and presentation pathway, and almost exclusively appeared on OP9-DL1 feeder cells (figure 2C–F and online supplemental figures S6,7).

Recent studies employing scRNAseq have identified new human DC populations and elucidated the heterogeneity of CD1c$^+$ DCs.[33–36 44–46] In our study, C3, 5, and 8 expressed *CD1C*, and C3 was notable for increased expression of cell cycle–associated genes (*MKI67*, *STMN1*, *CCNB1*, and *KPNA2*) (figure 2C and online supplemental figure S7) and pathway (figure 2F), consistent with mitotic DCs.[33] Expression of *CLEC10A*, the hallmark peripheral blood cDC2 gene, was low in C8; however, C8 exhibited higher levels of *CLEC4A*, *RUNX3*, *LTB*, *IL22RA2*, and *IDO1* resembling the cDC2A subset, recently identified in human spleen (figure 2D and online supplemental figure S7).[33] This subset was found mainly on OP9-DL1 feeder cells, and was notable for high expression of *CD3E*, which can be induced by Notch signaling.[47] C5 expressed higher levels of the canonical cDC2 markers, *CLEC10A* and *FCER1A*, suggesting cDC2Bs.[33]

To confirm the generation of cDC2A from iPSC-derived cells, we used scRNAseq data derived from a recent study by Brown *et al* evaluating Lin(CD3, CD56, CD19)$^-$CD14$^-$CD-11c$^+$HLA-DR$^+$ cells isolated from human spleen.[33] Using an integration-based approach, we projected DC subsets, C3, 5, 6, and 8, in our scRNAseq data onto the previously annotated cells reported by Brown *et al*[33] to generate a joint UMAP representation and infer DC cell states (figure 3 and online supplemental figure S8A). We found that iPSC-derived cells generated on OP9-DL1 feeder cells contained cDC1s and cDC2Bs and also cDC2As (figure 3B and online supplemental figure S8B). Consistent with these results, flow cytometric analysis of iPSC-derived CD16$^-$CD88$^-$CD141$^-$HLA-DR$^+$ cells identified CLEC4A^{hi}CLEC10A$^-$CD1c$^+$ cells representing cDC2A as well as CLEC4A^{lo}CLEC10A$^+$CD1c$^+$ cDC2B almost exclusively on OP9-DL1 feeder cells (figure 3C).

A previous report has shown that peripheral blood cDC2s contained CD5$^+$ and CD5$^-$ subsets with distinct gene expression and functions.[48] Also, high-dimensional single-cell analysis of PBMCs identified new DC subsets expressing *AXL* and *SIGLEC6*, named "AS-DCs".[36 44] In our study, CD163$^-$CD5$^+$CD1c$^+$ DCs (CD5$^+$cDC2s) and AS-DCs were only identified in iPSC-DCs on OP9-DL1 feeder cells on flow cytometric analysis (figure 3C and D and online supplemental figure 9). Consistent with this, we observed cells expressing *AXL*, *SIGLEC6*, and/or *CD5* within the DC clusters, C3, 5, 6, and/or 8 in our scRNAseq data (online supplemental figure 10A,B). Of note, there was an overlap between *CD5*-expressing cells and AS-DCs in our and Brown *et al*'s scRNAseq data (online supplemental figure 10C,D) in agreement with previous studies.[36 44 46]

CD1c$^+$ DCs expressing classical cDC2-related and monocyte-related genes have been identified, and named "DC3s".[36] DC3s are phenotypically defined as CD88$^-$ CD16$^-$CD163$^+$CD5$^-$ CD1c$^+$ with low to high expression of CD14.[34 35 45 46] Flow cytometric analysis revealed that the majority of iPSC-derived DC3s were found on OP9 feeder cells unlike cDC1s, cDC2As, cDC2Bs, CD5$^+$cDC2s, and AS-DCs differentiated on OP9-DL1 cells (figure 3C). This is consistent with distribution of cells expressing *CD163*, *CD36*, *CD14*, and *F13A1* (online supplemental figure 11), which are highly positive on DC3.[36] However, there were few cells co-expressing *CDKN1A* and *LMNA*, genes which are selectively expressed to higher levels in DC3s,[35] and some cells may also have expressed *C3AR1* and/or *C5AR1* encoding CD88, which are positive on monocytes, monocyte-derived DCs, and macrophages but negative on cDC2s and DC3s.[34–36] To clarify this issue, we projected our scRNAseq data onto the previously annotated cells reported by Villani *et al*, Bourdely *et al*, and Dutertre *et al* to confirm the presence of iPSC-derived DC3s. Using a reference map and cell annotations derived from Villani *et al* (online supplemental figure 12A), we found that a distinct subset of DC3s could be identified when projecting total cells (online supplemental figure 12B) but not DC clusters C3, 5, 6, and 8 (online supplemental figure 12C). Single-cell enrichment scores using the gene set specific to DC3 cells determined by Villani *et al* were

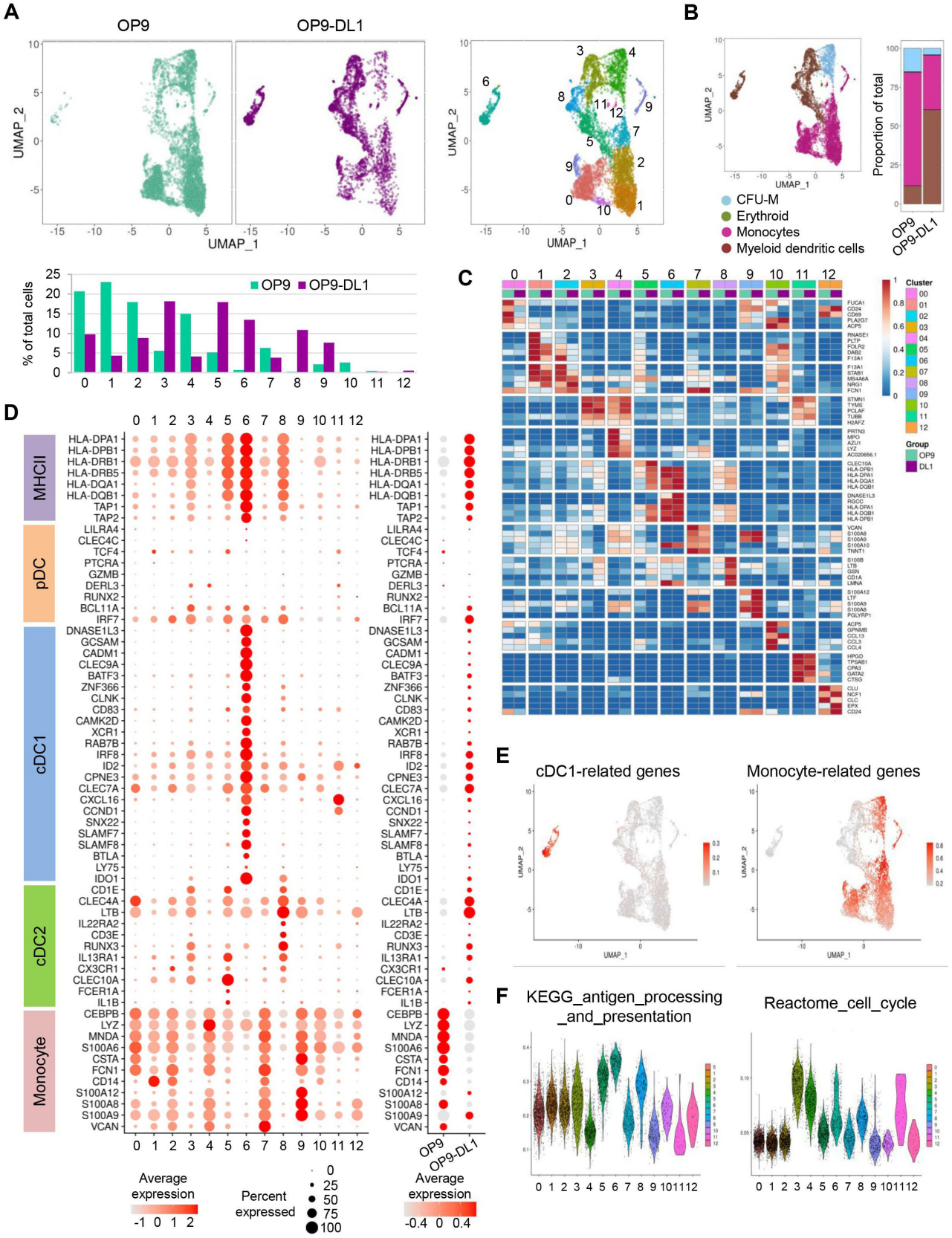

Figure 2 Identification of human iPSC-derived cDCs differentiated on OP9-DL1 cells by single-cell RNA sequencing. (A) UMAP plots of human iPSC-derived HLA-DR$^+$ cells differentiated cells on OP9 and OP9-DL1 cells. Frequency of each cluster is shown. (B) Distribution of computationally predicted cell types determined by SingleR using the Novershtern Hematopoietic reference. (C) Heatmap displaying mean normalized expression of selected genes in each cluster. (D) Raindrop plots displaying mean normalized expression of selected genes in each cluster. (E) Single-cell enrichment scores of cDC1-related and monocyte-related genes shown in (D). (F) Violin plots of single-cell enrichment scores within each cluster.

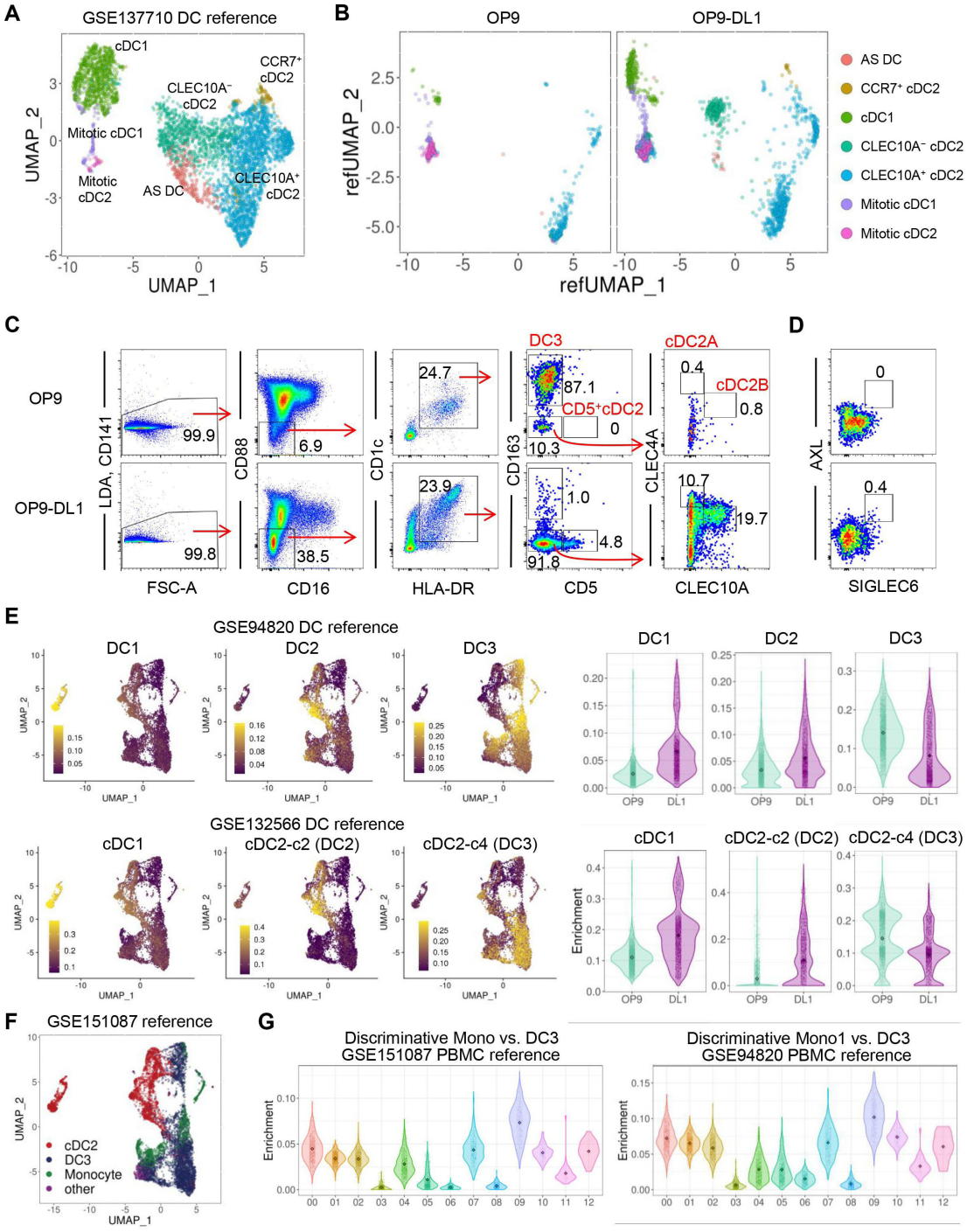

Figure 3 Heterogeneity of CD1c$^+$ DCs differentiated from human iPSCs. (A) UMAP plot of human Lin(CD3, CD56, CD19)$^-$ CD14$^-$CD11c$^+$HLA-DR$^+$ splenocytes from Brown *et al* (2020), colored by cell type. (B) UMAP plot of projecting clusters 3, 5, 6, and 8 from figure 2 of human iPSC-derived HLA-DR$^+$ cells differentiated on OP9 and OP9-DL1 cells projected onto human splenocyte atlas generated by Brown *et al* (2020). (C and D) Representative flow cytometric plots showing marker expression of human iPSC-derived cells on OP9 (upper) and OP9-DL1 (lower) feeder cells. Data shown are representative of two independent experiments. LDA, Live/Dead Aqua. (E) UMAP plots of single-cell enrichment scores using gene sets for specific DC subtypes derived from Villani *et al* (2017) (upper: Lin(CD3, CD56, CD19)$^-$HLA-DR$^+$CD11c$^+$CD14$^-$) and Dutertre *et al* (2019) (lower: cDC1: Lin(CD3, CD19, CD20)$^-$CD141$^+$CD14$^-$CD5$^-$CD123$^-$CD1c$^-$HLA-DR$^+$ cells, cDC2-c2: Lin$^-$CD14$^-$CD1c$^+$ cells, cDC2-c4: Lin$^-$CD14$^+$CD1c$^+$ cells). Violin plots show cell type score distributions in human iPSC-derived HLA-DR$^+$ cells differentiated on OP9 and OP9-DL1 cells. (F) UMAP plot showing cell type predictions of total cells from figure 2 of human iPSC-derived HLA-DR$^+$ cells differentiated on OP9 and OP9-DL1 cells derived from projection onto human PB CD16$^-$CD123$^-$CD141$^-$CD14$^{+/-}$CD1c$^+$ cell atlas generated by Bourdely *et al* (2019), colored by cell type. (G) Violin plots showing single-cell enrichment scores in each cluster from total cells in figure 2 using discriminative gene sets differentiating PB CD14$^+$CD16$^-$ monocytes compared with DC3 cells. Gene signatures were derived from direct comparisons of annotated clusters by Bourdely *et al* (2019) (Mono vs DC3, left) and by Villani *et al* (2017) (Mono1 vs DC3, right).

elevated in OP9 feeder cell group cells, with clusters C3, 5, 6, and 8 showing minimal DC3 enrichment (figure 3E and online supplemental figure 12D). Consistent with this, we found that enrichment scores using the gene set specific to DC3 cells determined from PB Lin(CD3/CD19/CD20)$^-$HLA-DR$^+$ cell analysis by Dutertre *et al* were also elevated in OP9 feeder cell group cells (figure 3E). Furthermore, using a reference map generated from PB CD16$^-$CD123$^-$CD141$^-$CD14$^{+/-}$ CD1c$^+$ cells by Bourdely *et al* (online supplemental figure 13A), we inferred cell types and determined populations of DC3 and monocytes (online supplemental figure 13B,C). On projecting total cells from our scRNAseq data onto the Bourdely *et al* reference map and computationally inferring cell states, we found markedly increased DC3 cells in iPSC-DCs differentiated on OP9 cells compared with OP9-DL1 cells while moderate overlap between DC3s and monocytes was observed (figure 3F and online supplemental figure 13D). Of note, this reference map was generated without PB cDC1s; therefore, iPSC-derived cDC1 was annotated as cDC2 in the figure 3F likely due to their expression of CD1c (figure 1D). Using gene sets differentiating monocyte populations from DC3 reported by Bourdely *et al* and Villani *et al*, we assessed single-cell enrichment scores and found there were differences of monocyte-related versus DC3-related gene expression among C0, 1, 2, 7, 9, 10, and 12 (figure 3G) initially annotated as monocytes (figure 2B).

Of note, we evaluated expression of plasmacytoid DC (pDC)–specific genes[11 20] including *GZMB*, *PTCRA*, *LILRA4*, *CLEC4C*, and *RUNX2*, but did not identify any distinct cluster of pDCs (figure 2D). To confirm this, we used a multimodal reference atlas of the human PBMCs reported by Hao *et al*.[49] We projected total cells in our scRNAseq data onto the previously annotated cells reported by Hao *et al*[49] to generate a joint UMAP representation and infer immune cell states (online supplemental figure 14A). From this analysis, we confirmed there were no pDCs identified either on OP9 or OP9-DL1 cells (online supplemental figure 14B,C). In agreement with this, flow cytometric analysis of iPSC-derived CD16$^-$HLA-DR$^+$ cells identified CD123$^+$CD303$^+$ population, the majority of which, however, were not CD45RA$^+$CD11c$^-$CX3CR1$^-$CD33$^-$ pDCs (online supplemental figure 15A). Some CD123$^+$CD303$^+$ cells contained CD45RA$^+$CD33$^+$CX3CR1$^+$CD2$^+$ cells resembling a subset, recently identified as pre-DCs (online supplemental figure 15B).[44] Taken together, our findings demonstrate a critical role of Notch signaling in regulating developmental pathway of human cDCs.

Notch signaling is required for differentiation of human iPSCs into cDC1s, cDC2s, AS-DCs but not DC3

Having identified cDC1-like cells in human iPSC-derived HLA-DR$^+$ cells differentiated on OP9-DL1 but not OP9 cells by conventional flow cytometry and scRNAseq, we employed a loss-of-function approach using a γ-secretase inhibitor, DAPT,[20] to verify the role of Notch signaling in generation of cDC1s from human iPSCs. This inhibitor blocks the Notch signaling pathway by inhibiting the last proteolytic step before the release of Notch1 intracellular domain (NICD1), which is essential for Notch activation. Human iPSC-derived CD34$^+$ cells were cultured on OP9 or OP9-DL1 cells in the presence or absence of DAPT, and iPSC-derived HLA-DR$^+$ cells were characterized by flow cytometry. We found that addition of DAPT markedly decreased the generation of cDC1-like cells and AS-DCs differentiated on OP9-DL1 cells (figure 4A and online supplemental figure 16). Furthermore, inhibition of Notch signaling substantially decreased cDC2 subsets CLEC4A^{hi}CLEC10A$^-$ (cDC2A), CLEC4A^{lo}CLEC10A$^+$ (cDC2B), and CD5$^+$CD163$^-$ (CD5$^+$ cDC2) but increased CD5$^-$CD163$^+$ CD1c$^+$HLA-DR$^+$ DCs (DC3) (figure 4B). Thus, these results demonstrate that Notch signaling is required for in vitro differentiation of human iPSCs to cDC1-like cells, AS-DCs, cDC2As, cDC2Bs, and CD5$^+$cDC2s but not DC3s.

Notch-activated iPSC-derived CD141$^+$XCR1$^+$CLEC9A$^+$ DCs and human peripheral blood cDC1s display similar gene expression profile

Previous studies have shown the generation of CD141$^+$XCR1$^+$ DCs from human iPSCs under feeder-free and xeno-free conditions without Notch signaling.[19] Now that human iPSCs can be derived and maintained under feeder-free and xeno-free conditions, this approach might allow us to generate cDCs from human somatic cells under defined feeder-free and xeno-free conditions. In this protocol, human iPSCs were cultured with a cocktail of cytokines including GM-CSF, SCF, VEGF, BMP4, and IL-4 without xeno-components under defined conditions. In our hands, we added Flt3L to this protocol and found that human iPSCs differentiated into CD141$^+$XCR1$^+$CLEC9A$^+$HLA-DR$^+$ cells (online supplemental figure 17A–C). Of note, HLA-DR$^+$ cells differentiated from TiPSCs did not express T-cell receptor α/β (online supplemental figure 18).

At this point, we found cDC1-like cells expressing CD141, XCR1, and CLEC9A were generated from human iPSCs with or without xenogeneic feeder cells; however, similarities of gene expression between human iPSC-derived cDC1-like cells and peripheral blood cDC1s remain unknown. To further explore the effect of DL1-Notch signaling on in vitro human iPSC-derived DCs, we flow-sorted XCR1$^+$CLEC9A$^+$HLA-DR$^+$CD11c$^+$ cells differentiated from on-feeder and feeder-free culture conditions (hereafter referred to as DL1-iPSC-cDC1s or FF-iPSC-cDC1s, respectively), and interrogated their expression profiles by global mRNA sequencing (RNAseq). Peripheral blood XCR1$^+$CLEC9A$^+$HLA-DR$^+$CD11c$^+$ cells (PB-cDC1s) were used as a control.

To determine relationships between PB-cDC1s, DL1-iPSC-cDC1s, and FF-iPSC-cDC1s, we performed hierarchical clustering of all 2748 differentially expressed genes (DEGs; fold change >1.5, fdr adjusted p value<0.05) identified between groups and visualized expression patterns

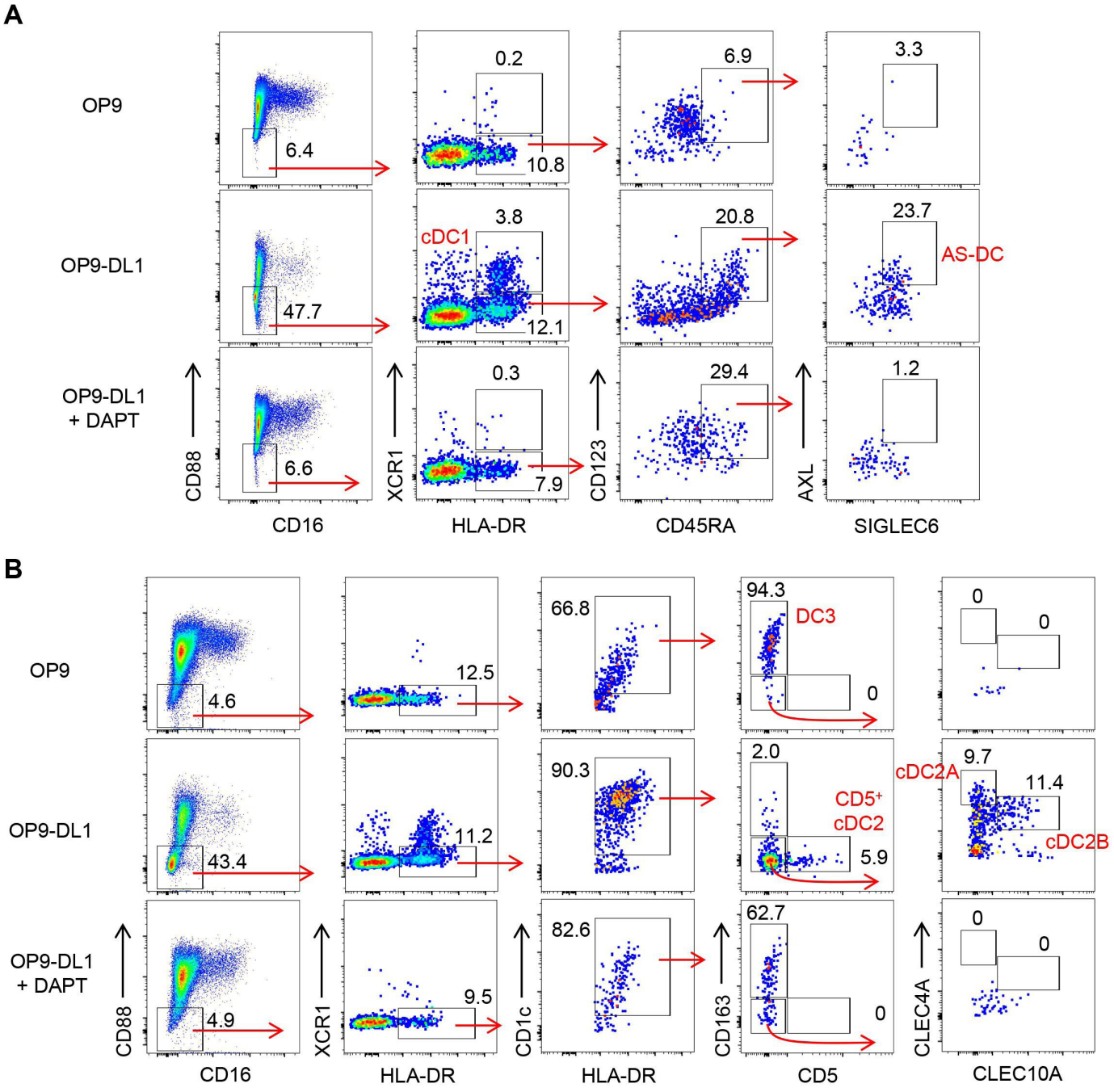

Figure 4 Notch signaling is required for generation of cDCs from human iPSCs. (A, B Human iPSCs were differentiated on OP9 or OP9-DL1 cells in the presence or absence of a γ-secretase inhibitor, N-[N-(3,5-difluorophenacetyl)- L-alanyl]-S-phenylglycine t-butyl ester (DAPT). The gating strategy and frequency of XCR1$^+$HLA-DR$^+$cDC1s and AS-DCs (A) and various CD1c$^+$HLA-DR$^+$ DCs: CLEC4A^{hi}CLEC10A$^-$ (cDC2A), CLEC4A^{lo}CLEC10A$^+$ (cDC2B), CD5$^+$CD163$^-$ (CD5$^+$ cDC2), and CD5$^-$CD163$^+$ (DC3) (B) are shown.

using a dendrogram and a heat map (figure 5A). The clustering pattern indicates that the replicates of DL1-iPSC-cDC1s and PB-cDC1s share similar transcriptional patterns. However, FF-iPSC-cDC1s are transcriptionally distinct from DL1-iPSC-cDC1s and PB-cDC1s. Similarly, PCA indicated that a major proportion of variation in transcriptional states across samples could be explained by the source of cDC1 isolation and further demonstrated that PB-cDC1s are more closely related to DL1-iPSC-cDC1s than to FF-iPSC-cDC1s (figure 5B). Concordance of DEGs between the three groups is represented by a Venn diagram (figure 5C). We found markedly more DEGs between FF-iPSC-cDC1s and DL1-iPSC-cDC1s (1678 DEGs) or PB-cDC1s (2200 DEGs) compared with between DL1-iPSC-cDC1s and PB-cDC1s (213 DEGs) (figure 5C). Volcano plots for FF-iPSC-cDC1s versus PB-cDC1s showed cDC1-related genes including *CLEC9A*, *IDO1*, *XCR1*, and *CADM1* are significantly reduced while the expression of these genes was similar between DL1-iPSC-cDC1s and PB-cDC1s (figure 5D). We further evaluated DEGs

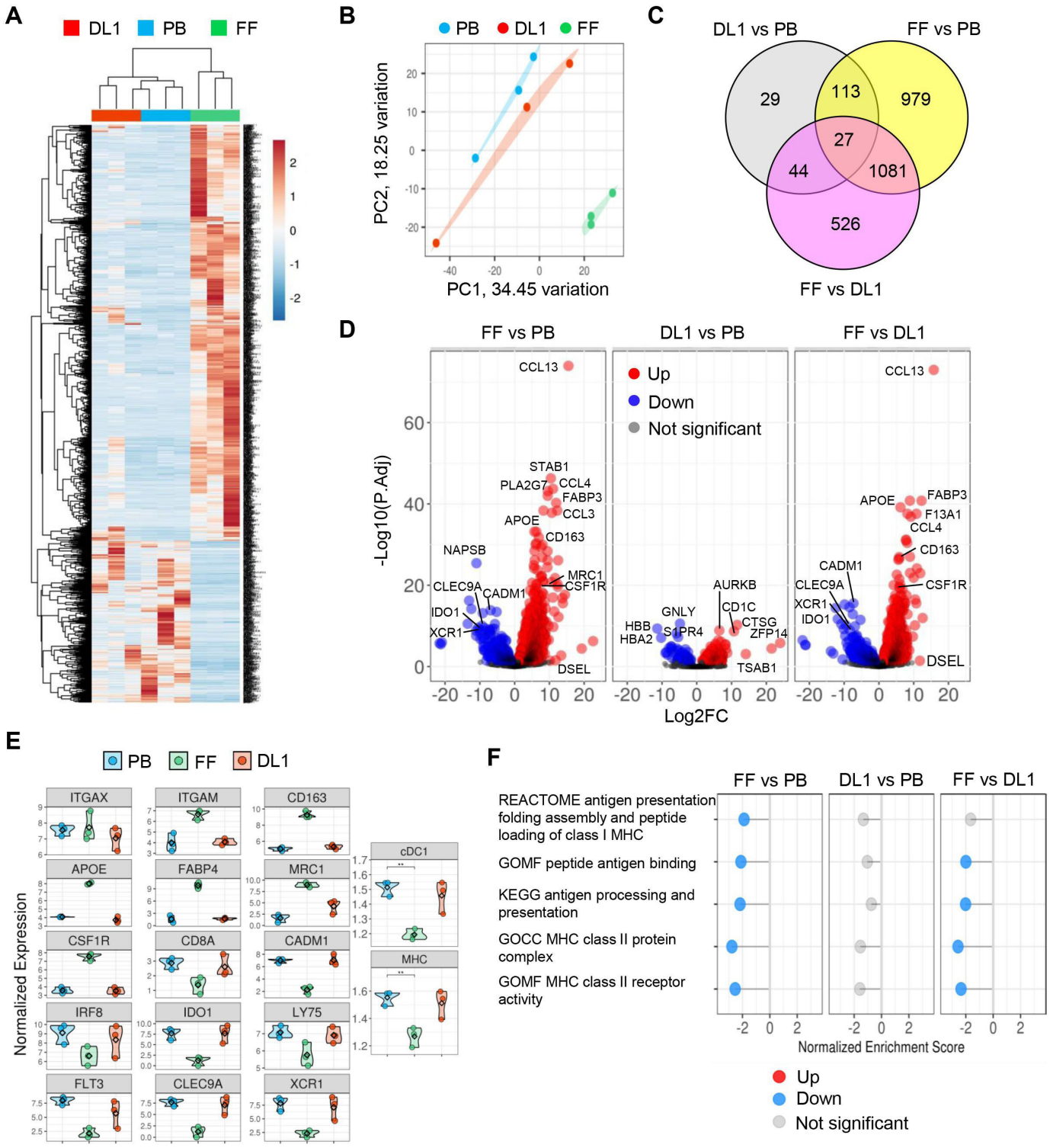

Figure 5 Notch-activated human iPSC-derived CD141$^+$XCR1$^+$CLEC9A$^+$ DCs and human peripheral blood cDC1s display similar gene expression profile. (A) Heat map representing genes differentially expressed between XCR1$^+$CLEC9A$^+$HLA-DR$^+$CD11c$^+$ cells differentiated on OP9-DL1 cells (DL1) or under feeder-free (FF) condition, or in peripheral blood (PB). (B) Principal component analysis (PCA). (C) Venn diagram of differentially expressed genes in DL1, FF, and PB XCR1$^+$CLEC9A$^+$HLA-DR$^+$CD11c$^+$ cells. (D–F) Volcano plot (D), representative gene expression (E), and gene set enrichment analysis (GSEA) (F) of DL1, FF, and PB XCR1$^+$CLEC9A$^+$HLA-DR$^+$CD11c$^+$ cells.

between groups and found that although *ITGAX* gene, encoding for the CD11c protein, was similarly expressed in all groups, DL1-iPSC-cDC1s and PB-cDC1s expressed higher levels of cDC1-related and MHC-related genes than FF-iPSC-cDC1s (figure 5E). In contrast, genes associated with monocytes/macrophages such as *ITGAM*, *CD163*, *APOE*, *FABP4*, *MRC1*, and *CSF1R* were higher in FF-iPSC-cDC1s. Accordingly, DL1-iPSC-cDC1s and

PB-cDC1s were notable for high levels of pathways related to MHC class II, and antigen processing and presentation compared with FF-iPSC-cDC1s (figure 5F). Together, DL1-Notch signaling allows human iPSCs to differentiate to peripheral blood cDC1-like cells in vitro.

Phagocytic, T-cell proliferative, and cytokine-producing capacities of DL1-iPSC-DCs

To gain insights into the function of iPSC-cDCs, we evaluated the capacity of iPSC-DCs differentiated on OP9-DL1 feeder cells to phagocytose antigen and activate T cells. The phagocytic capacity of human iPSC-DCs was measured by amounts of cellular absorption of pHrodo zymosan particles, which become fluorescent once at acidic pH such as in phagosomes. We found that pHrodo zymosan particles were efficiently phagocytosed by human iPSC-derived cells (figure 6A), and iPSC-derived cDC1s, cDC2As, cDC2Bs, and DC3s demonstrated comparable phagocytic ability (figure 6B–D). We also evaluated the phagocytic ability of FF-iPSC-cDC1s and found that many FF-iPSC-cDC1s were not viable after phagocytosis of zymosan particles (online supplemental figure 19A,B).

We next tested whether human iPSC-DCs could enhance proliferation of T cells. To this end, we co-cultured human iPSC-DCs with isolated T cells from the same donor in the presence of MHC class I or II peptides specific to various viruses and IL-2. Human iPSC-DCs differentiated on OP9-DL1 cells facilitated proliferation of $CD8^+$ and $CD4^+$ T cells in the presence of MHC class I and II peptides, respectively (figure 7A). We found that both proliferating T cells effectively downregulated CD62L and CD45RA, and upregulated CD25 (figure 7B). Small populations of proliferating $CD8^+$ and $CD4^+$ T cells maintain the expression of CD45RA, CD62L, and CD27, suggesting less-differentiated T cells (figure 7C). Furthermore, flow-sorted $CLEC9A^+$ DL1-iPSC-cDC1s induced proliferation of $CD8^+$ T cells in the presence of MHC class I peptides (figure 7D).

Lastly, we evaluated cytokine-producing capacity of iPSC-DCs. DL1-iPSC-cDC1s, cDC2As, cDC2Bs, and OP9-iPSC-DC3 produced IL-12 and TNF-α on stimulation with TLR agonists, poly(I:C), R848, LPS, and CpG (figure 8A). IFN-λ was secreted by DL1-iPSC-cDC1s while negligible IFN-α was produced by either OP9-iPSC-DCs or DL1-iPSC-DCs (figure 8B and C). Collectively, human iPSCs could differentiate into various functional cDC subsets in vitro.

DISCUSSION

In this study, we demonstrated generation of cDC-like cells from human iPSCs. Key results described herein include (1) Notch-signaling dependent efficient in vitro differentiation of human iPSCs into $CD141^+XCR1^+CLEC9A^+HLA\text{-}DR^+$ cells resembling PB cDC1s; (2) generation of various cDC subsets but not pDCs from human iPSCs; (3) identification of the heterogeneity of human iPSC-derived cDCs including cDC2A, cDC2B, $CD5^+cDC2^+$, DC3, and AS-DC subsets (online supplemental figure 20); and (4) phagocytic, T cell proliferative, and cytokine-producing capacities of human iPSC-derived cDC-like cells.

Recent evidence suggests Notch-signaling dependent differentiation of cDC1s from $CD34^+$ HSCs.[20 21] Our study is in line with this, and further demonstrated efficient generation of cDC1-like cells as well as various cDCs including cDC2As, cDC2Bs, $CD5^+$cDC2s, and AS-DCs from human iPSC-derived $CD34^+$ HPCs. Although these two recent studies have shown the generation of IFN-α-producing pDCs from human $CD34^+$ HSCs in co-culture with OP9 cells, we did not identify pDCs derived from human iPSCs co-cultured with either OP9 or OP9-DL1. The majority of $CD123^+CD303^+$ cells in both OP9 and OP9-DL1 feeder cells expressed myeloid markers such as CD11c, CD33, and/or CX3CR1. Consistent with this, IFN-α production was not detected on stimulation with TLR agonists including CpG. Additional work is needed to better understand the molecular and cellular mechanisms underlying the development of pDCs from human iPSCs.

High-dimensional, single-cell RNA expression analysis confirmed the generation of cDC1s and also probed the diversity of $CD1c^+$ DCs in human iPSC-derived cells. We found that human iPSCs could differentiate into cDC2As expressing *CLEC4A*, *RUNX3*, *LTB*, *IL22RA2*, and *IDO1*, recently identified in human spleen as well as canonical cDC2Bs expressing *CLEC10A* and *FCER1A*. Furthermore, human iPSC-derived DCs projected onto the reference human splenocyte map[33] confirmed the generation of cDC2As. Notably, human iPSC-derived cDC2As were only identified on OP9-DL1 but not on OP9 cells, suggesting a potential role of Notch signaling in generation of cDC2As as well as cDC1s. These findings are congruent with increased expression of genes related to Notch signaling in cDC2As in mouse and human spleen.[33] Evidence showed that cDC2As could be isolated from human spleen but not peripheral blood.[33] This suggests that Notch signaling-mediated differentiation of human iPSCs allows us to generate primary cDC that may not be obtained from leukapheresis.

Our loss-of-function approach with a γ-secretase inhibitor for blocking Notch signaling provided mechanistic insight into the differentiation of other $CD1c^+$ DC subsets. Addition of a γ-secretase inhibitor in an OP9-DL1 feeder system substantially decreased the frequency of cDC2Bs and $CD5^+$cDC2s, suggesting that Notch signaling may also have an important role in differentiation of cDC2Bs and $CD5^+$ cDC2s. In contrast, DC3s were differentiated either on OP9 or OP9-DL1 feeder cells, and increased with a γ-secretase inhibitor. This indicates that development of DC3 subset is independent of that of cDC1s and cDC2s in line with a recent work showing that DC3s do not differentiate via cDC-restricted common DC precursor (CDP).[34 45] Moreover, our results of increased frequency of CDP-derived DCs but decreased frequency of DC3s on OP9-DL1 feeder cells suggest that Notch signaling

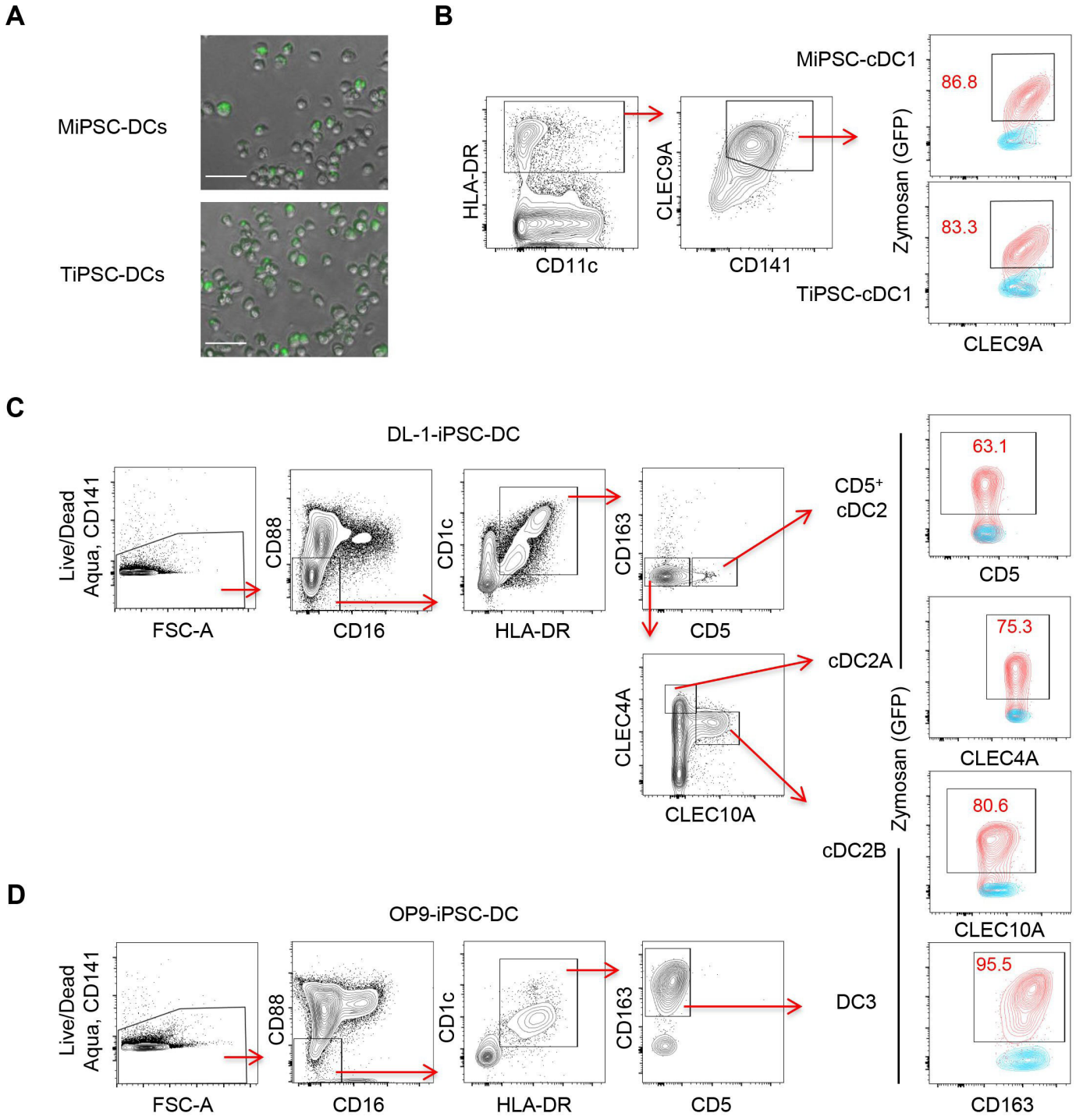

Figure 6 Phagocytic capacity of human iPSC-derived DCs. (A) Representative pictures of human iPSC-derived cells in co-culture with pHrodo zymosan particles. MiPSC, monocyte-derived iPSC; TiPSC, T cell–derived iPSC (scale bar, 50 µm). (B, C) Representative histogram showing zymosan expression in human iPSC-derived cDC1s (B), CD5$^+$ cDC2s, cDC2As, cDC2Bs (C), and DC3s (D) differentiated on OP9-DL1 (B, C) or OP9 cells (D). Data shown are representative of two independent experiments.

orchestrates the reciprocal development of these two distinct DC lineages. Nonetheless, data presented herein underscore that human iPSCs offer unique advantages for developmental studies.[50 51] More work is needed to delineate the mechanisms underlying the potential lineage decisions of cDC2s and DC3s.

Recent advances in single-cell molecular profiling have made it possible to identify various rare DC subsets including AS-DCs in peripheral blood.[36 44] The use of reference dataset relevant to the study of interest also improves the accuracy of cell-type classification and allows cell-type discovery in the sample without enrichment

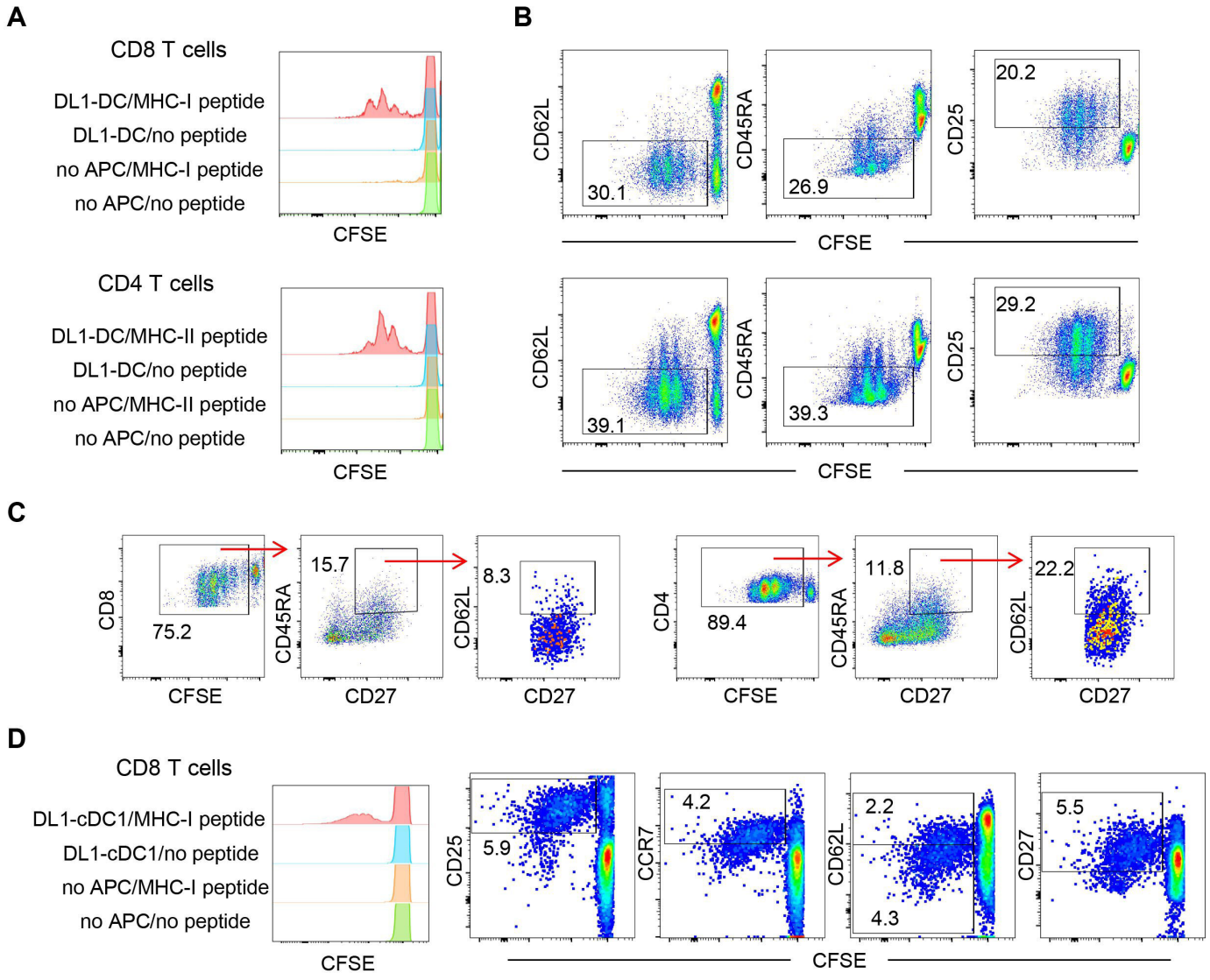

Figure 7 T-Cell proliferative capacity of human iPSC-derived DCs. (A) Representative histogram showing CFSE expression in peripheral blood T cells co-cultured with or without DL-1-iPSC-DCs in the presence or absence with MHC class I or II peptides in vitro. (B, C) Representative flow cytometric plots showing CFSE-labeled peripheral blood T cells from (A). (D) Representative histogram and flow cytometric plots showing CFSE expression in peripheral blood T cells co-cultured with or without DL-1-iPSC-CLEC9A$^+$ DCs in the presence or absence with MHC class I peptides in vitro. Data shown are representative of two independent experiments.

of rare cell types prior to scRNAseq.[33] In this study, projecting our scRNAseq data onto the reference human splenocyte atlas helped identify AS-DC and cDC2As as well as confirm the presence of DC3 in human iPSCs-derived HLA-DR$^+$ cells. In addition, we found gene-expression profiling was necessary to determine a cell type in this study. Human iPSCs differentiated under feeder-free and xeno-free conditions without Notch signaling expressed cDC1 markers; however, bulk RNAseq analysis revealed that the transcriptomic landscape of CD141$^+$XCR1^{+-} CLEC9A$^+$HLA-DR$^+$ cells generated under this condition markedly differed from DL1-iPSC-cDC1s and PB-cDC1s. Collectively, our study illustrates the significance of combining omics approaches and systems biology with conventional flow cytometric analysis in interrogating the heterogeneity and development of human iPSC-derived myeloid cells.

Our study has some limitations. More work is warranted to determine the function of each human iPSC-derived DC subset. For example, cDC1s specialize in cross-presentation and priming CD8$^+$ T cells for tumors and pathogens that do not directly infect DCs[52–54]; however, cross-priming capacity of human iPSC-derived cDC1s remains unknown. Our study is limited to assessing in vitro functions of iPSC-derived cDCs. Although subsets of iPSC-derived cDCs expressed CCR7, their migratory potential remains elusive. Similarly, whether iPSC-derived cDCs exhibit the ability to phagocytose tumor antigens in the immunosuppressive tumor microenvironment remains an open question. We found DL1-iPSC-cDC1s

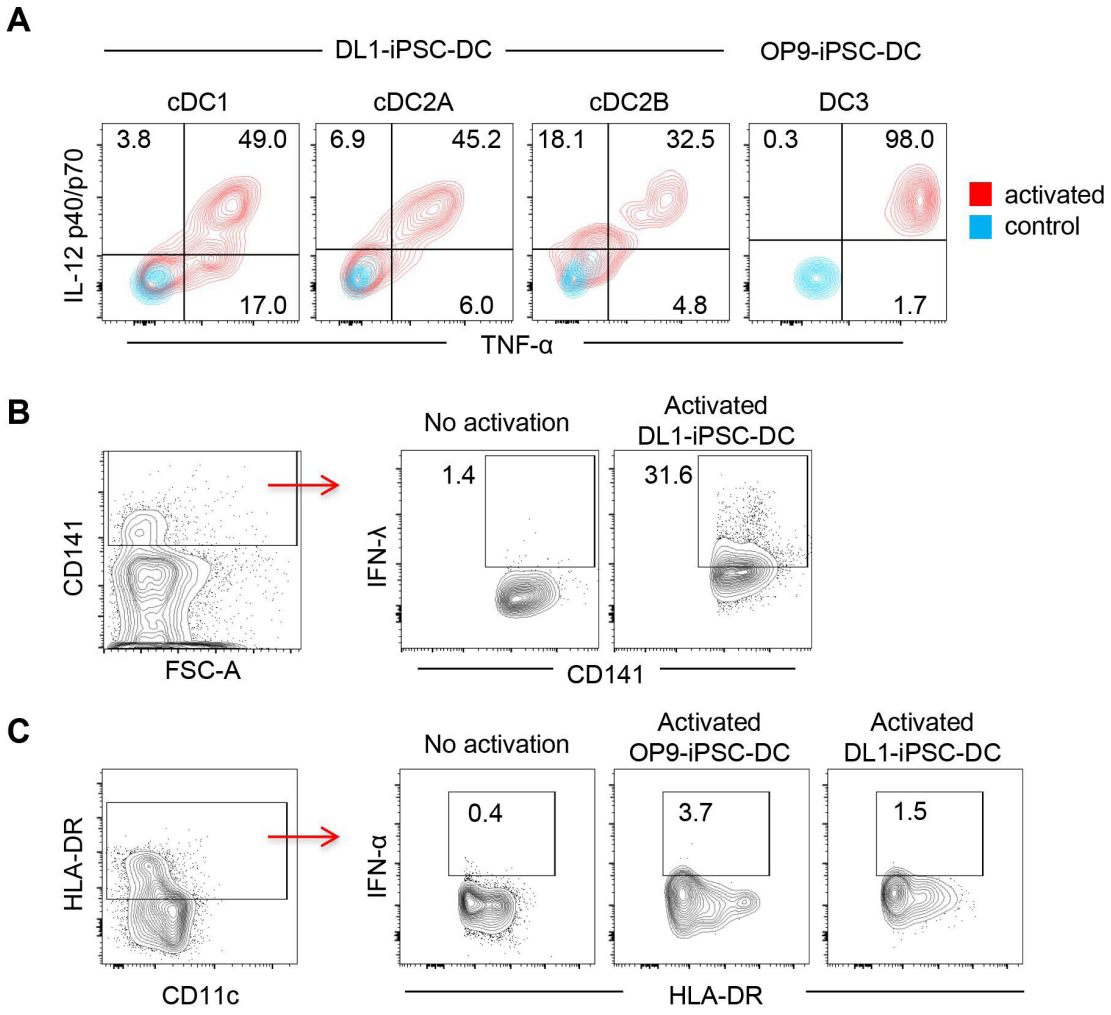

Figure 8 Cytokine-producing capacity of human iPSC-derived DCs. (A–C) IL-12p40/p70 (A), TNF-α (A), IFN-λ (B), and IFN-α (C) production on stimulation with TLR agonists, poly(I:C), R848, LPS, and CpG by human iPSC-derived DCs differentiated on OP9 (A, C) or OP9-DL1 (A–C) cells. cDC1: $CD16^-CD88^-CLEC10A^-CLEC9A^+HLA\text{-}DR^+$ cells. cDC2A: $CD16^-CD88^-CD141^-CLEC10A^-CLEC4A^{hi}CD1c^+HLA\text{-}DR^+$ cells. cDC2B: $CD16^-CD88^-CD141^-CLEC10A^+CLEC4A^{lo}CD1c^+HLA\text{-}DR^+$ cells. DC3: $CD16^-CD88^-CD141^-$ $CD163^+CD1c^+HLA\text{-}DR^+$ cells. Data shown are representative of two independent experiments.

expressed CD1c as observed in $CD141^+$ cDC1s differentiated from human $CD34^+$ cord blood progenitors in vitro and in Flt3L-induced $CD141^+$ cDC1s in vivo.[20 42 43] Developmental process from double-positive $CD1c^+CD141^+$ cDC1s to $CD141^+$ cDC1s remains unknown. Our findings suggest a role of Notch signaling in differentiation of $CD5^+$ cDC2s and AS-DCs on flow cytometric analyses. However, confirmation of this was limited due to the rarity of this subset in our scRNAseq data. Expression of CD5, AXL, and SIGLEC6 has been found in DC precursors,[44] and evaluation of DC differentiation at different stages of human iPSC-derived cells might elucidate ontogeny and developmental pathway of $CD5^+$ cDC2s and AS-DCs. Our scRNAseq analyses and others have identified the presence of "mitotic DCs" with higher expression of cell cycle–related genes in human iPSC-derived DCs and spleen,[33] respectively. However, it remains unclear whether this cell population maintains the ability to proliferate. We aimed to generate cDC1s from human iPSCs and used Flt3L which is critical to development of DCs. Although the scope of this study was limited to determining Notch signaling for the development of cDC1s, one future area of investigation is to decipher growth factor requirements for the development of cDC1s as well as other DC subsets from human iPSCs. Lastly, potential tumorigenicity of iPSC-derived cDCs needs to be evaluated before this approach is clinically translated in the clinic.

Despite promising immunogenicity and favorable safety profiles, DC-based immunotherapies have elicited only limited clinical responses.[5 7] One possible explanation for this is that DCs differentiated from peripheral blood monocytes in the presence of GM-CSF and IL-4 have less adjuvant capacity and immune-activating properties such as antigen-presentation capabilities due to lower MHC molecule expression compared with bona fide DC subsets.[5 7] Clinical efforts using naturally circulating primary DCs are underway although they are relatively scarce.[7] While clinical translational potential of iPSC-cDCs remains to be determined, one possible way to use them would be intratumoral injection. The frequency of cDC1s

in the tumor correlates with prognosis and response to anti-PD-1/PD-L1 therapy,[14] and in situ injection or mobilization of cDCs enhances response to anti-PD-1/PD-L1 therapy and immunogenicity of radiotherapy in preclinical models and patients.[55–59] Regarding this, we have recently reported antitumor efficacy of multimodal intralesional therapy with in situ delivery of mouse iPSC-DC and radiation therapy against preclinical models of breast cancer resistant to anti-PD-L1 therapy.[56] Future studies with humanized mouse models where MHC is matched between human iPSC-DCs and engrafted PBMCs or $CD34^+$ cells are expected to provide insight into in vivo therapeutic efficacy of human iPSC-DCs compared with bona fide and monocyte-derived DCs. Considering the clinical application of human iPSC-derived cDCs, the use of recombinant human delta-like 1-Fc antibody[60] might provide the opportunity to generate cDCs from human iPSCs under feeder- and xeno-free conditions.

In summary, we reported in vitro methods to efficiently differentiate human iPSCs to $CD141^+XCR1^+CLEC9A^+$ DCs resembling PB-cDC1s. Loss-of-function and gain-of-function studies unraveled the role of Notch signaling in regulating generation of cDCs from human iPSCs. Single-cell profiling of human iPSC-derived DCs confirmed a cluster expressing high levels of cDC1 signature and revealed the heterogeneity of $CD1c^+$ DCs that warrants further investigation. Our work provides a solid foundation for the future development of personalized treatment with unlimited numbers of autologous $CD141^+XCR1^{+-}CLEC9A^+$ DCs from human iPSCs in the clinic.

Author affiliations
[1]Center for Immunotherapy, Roswell Park Comprehensive Cancer Center, Buffalo, New York, USA
[2]Department of Obstetrics and Gynecology, Akita University Graduate School of Medicine School of Medicine, Akita, Japan
[3]Department of Biostatistics and Bioinformatics, Roswell Park Comprehensive Cancer Center, Buffalo, New York, USA
[4]Department of Surgery, Shinshu University Graduate School of Medicine School of Medicine, Matsumoto, Nagano, Japan
[5]Department of Pathology, Roswell Park Comprehensive Cancer Center, Buffalo, New York, USA
[6]Department of Immunology, Roswell Park Comprehensive Cancer Center, Buffalo, New York, USA
[7]Department of Surgical Oncology, Roswell Park Comprehensive Cancer Center, Buffalo, NY, USA
[8]Department of Surgery, University of Southern California, Los Angeles, CA, USA

Twitter Fumito Ito @lab_ito

Acknowledgements We acknowledge Prometheus Laboratories Inc. for kindly providing recombinant human IL-2 and BioRender.com for illustrations. We thank Drs. Anm Nazmul Khan, Takayoshi Yamauchi, and Kumiko Iwabuchi (Roswell Park Comprehensive Cancer Center) for technical assistance.

Contributors KM designed and performed experiments, analyzed data, and wrote the manuscript. ML contributed the bioinformatics analyses and revised the article. RK, SM, and TO performed experiments, and revised the article. KK performed pathologic examination of tissue samples and revised the article. SL supervised the bioinformatics analyses and revised the article. FI developed the concept, analyzed data, managed the project, coordinated author activities, revised the article, provided final approval of the version to be submitted, and is responsible for the overall content as the guarantor,

Funding This work was supported by National Cancer Institute (NCI) grant P30CA016056 involving the use of Roswell Park's Flow and Image Cytometry, Bioinformatics, and Genomic Shared Resources. This work was supported by the Melanoma Research Alliance and the Sarcoma Foundation of America (FI), Uehara Memorial Foundation (TO), and National Cancer Institute (NCI) grant, U24CA232979 (ML and SL), K08CA197966, and R01CA255240-01A1 (FI).

Competing interests None declared.

Patient consent for publication Consent obtained directly from a healthy volunteer

Ethics approval This study involves human participants and was approved by the Institutional Review Board (IRB) of Roswell Park Comprehensive Cancer Center (protocol # BDR072916) and the University at Buffalo/Roswell Park Stem Cell Research Oversight (SCRO) Committee (protocol #17-001-RP), and has been performed in accordance with the ethical standards of the responsible committee on human experimentation and with the Helsinki Declaration. An IRB-approved written informed consent was obtained from a healthy donor for being included in the study. Participants gave informed consent to participate in the study before taking part.

Provenance and peer review Not commissioned; externally peer reviewed.

Data availability statement Data are available on reasonable request. All data derived from RNA-seq and scRNA-seq studies are deposited at NCBI Gene Expression Omnibus under series accession GSE193488.

ORCID iD
Fumito Ito http://orcid.org/0000-0002-6866-671X

REFERENCES

1 Banchereau J, Palucka AK, Dhodapkar M, *et al*. Immune and clinical responses in patients with metastatic melanoma to CD34(+) progenitor-derived dendritic cell vaccine. *Cancer Res* 2001;61:6451–8.
2 Palucka K, Banchereau J. Cancer immunotherapy via dendritic cells. *Nat Rev Cancer* 2012;12:265–77.
3 Wculek SK, Cueto FJ, Mujal AM, *et al*. Dendritic cells in cancer immunology and immunotherapy. *Nat Rev Immunol* 2020;20:7–24.
4 Luo X-L, Dalod M. The quest for faithful in vitro models of human dendritic cells types. *Mol Immunol* 2020;123:40–59.
5 Saxena M, Balan S, Roudko V, *et al*. Towards superior dendritic-cell vaccines for cancer therapy. *Nat Biomed Eng* 2018;2:341–6.
6 Perez CR, De Palma M. Engineering dendritic cell vaccines to improve cancer immunotherapy. *Nat Commun* 2019;10:5408.
7 Bol KF, Schreibelt G, Rabold K, *et al*. The clinical application of cancer immunotherapy based on naturally circulating dendritic cells. *J Immunother Cancer* 2019;7:109.
8 Osugi Y, Vuckovic S, Hart DNJ. Myeloid blood CD11c(+) dendritic cells and monocyte-derived dendritic cells differ in their ability to stimulate T lymphocytes. *Blood* 2002;100:2858–66.
9 Balan S, Ollion V, Colletti N, *et al*. Human XCR1+ dendritic cells derived in vitro from CD34+ progenitors closely resemble blood dendritic cells, including their adjuvant responsiveness, contrary to monocyte-derived dendritic cells. *J Immunol* 2014;193:1622–35.
10 Wculek SK, Amores-Iniesta J, Conde-Garrosa R, *et al*. Effective cancer immunotherapy by natural mouse conventional type-1 dendritic cells bearing dead tumor antigen. *J Immunother Cancer* 2019;7:100.

11 Robbins SH, Walzer T, Dembélé D, *et al*. Novel insights into the relationships between dendritic cell subsets in human and mouse revealed by genome-wide expression profiling. *Genome Biol* 2008;9:R17.
12 Shortman K, Heath WR. The CD8+ dendritic cell subset. *Immunol Rev* 2010;234:18–31.
13 Hildner K, Edelson BT, Purtha WE, *et al*. Batf3 deficiency reveals a critical role for CD8α+ dendritic cells in cytotoxic T cell immunity. *Science* 2008;322:1097–100.
14 Broz ML, Binnewies M, Boldajipour B, *et al*. Dissecting the tumor myeloid compartment reveals rare activating antigen-presenting cells critical for T cell immunity. *Cancer Cell* 2014;26:638–52.
15 Roberts EW, Broz ML, Binnewies M, *et al*. Critical role for CD103(+)/CD141(+) dendritic cells bearing CCR7 for tumor antigen trafficking and priming of T cell immunity in melanoma. *Cancer Cell* 2016;30:324–36.
16 Senju S, Haruta M, Matsumura K, *et al*. Generation of dendritic cells and macrophages from human induced pluripotent stem cells aiming at cell therapy. *Gene Ther* 2011;18:874–83.
17 Choi K-D, Vodyanik MA, Slukvin II. Generation of mature human myelomonocytic cells through expansion and differentiation of pluripotent stem cell-derived lin-CD34+CD43+CD45+ progenitors. *J Clin Invest* 2009;119:2818–29.
18 Iizuka-Koga M, Asashima H, Ando M, *et al*. Functional analysis of dendritic cells generated from T-iPSCs from CD4+ T cell clones of Sjögren's syndrome. *Stem Cell Reports* 2017;8:1155–63.
19 Sachamitr P, Leishman AJ, Davies TJ, *et al*. Directed differentiation of human induced pluripotent stem cells into dendritic cells displaying tolerogenic properties and resembling the CD141$^+$ subset. *Front Immunol* 2017;8:8.
20 Balan S, Arnold-Schrauf C, Abbas A, *et al*. Large-scale human dendritic cell differentiation revealing Notch-dependent lineage bifurcation and heterogeneity. *Cell Rep* 2018;24:1902–15.
21 Kirkling ME, Cytlak U, Lau CM, *et al*. Notch signaling facilitates In vitro generation of cross-presenting classical dendritic cells. *Cell Rep* 2018;23:3658–72.
22 Saito H, Okita K, Fusaki N, *et al*. Reprogramming of melanoma tumor-infiltrating lymphocytes to induced pluripotent stem cells. *Stem Cells Int* 2016;2016:11
23 Seki T, Yuasa S, Oda M, *et al*. Generation of induced pluripotent stem cells from human terminally differentiated circulating T cells. *Cell Stem Cell* 2010;7:11–14.
24 Saito H, Iwabuchi K, Fusaki N, *et al*. Generation of induced pluripotent stem cells from human melanoma tumor-infiltrating lymphocytes. *J Vis Exp* 2016;117:1. doi:10.3791/54375
25 Nakagawa M, Taniguchi Y, Senda S, *et al*. A novel efficient feeder-free culture system for the derivation of human induced pluripotent stem cells. *Sci Rep* 2014;4:3594.
26 Okita K, Yamakawa T, Matsumura Y, *et al*. An efficient nonviral method to generate integration-free human-induced pluripotent stem cells from cord blood and peripheral blood cells. *Stem Cells* 2013;31:458–66.
27 Yamauchi T, Hoki T, Oba T, *et al*. T-cell CX3CR1 expression as a dynamic blood-based biomarker of response to immune checkpoint inhibitors. *Nat Commun* 2021;12:1402.
28 Butler A, Hoffman P, Smibert P, *et al*. Integrating single-cell transcriptomic data across different conditions, technologies, and species. *Nat Biotechnol* 2018;36:411–20.
29 Wolock SL, Lopez R, Klein AM. Scrublet: computational identification of cell doublets in single-cell transcriptomic data. *Cell Syst* 2019;8:281–91.
30 Tirosh I, Izar B, Prakadan SM, *et al*. Dissecting the multicellular ecosystem of metastatic melanoma by single-cell RNA-seq. *Science* 2016;352:189–96.
31 Aran D, Looney AP, Liu L, *et al*. Reference-based analysis of lung single-cell sequencing reveals a transitional profibrotic macrophage. *Nat Immunol* 2019;20:163–72.
32 Novershtern N, Subramanian A, Lawton LN, *et al*. Densely interconnected transcriptional circuits control cell states in human hematopoiesis. *Cell* 2011;144:296–309.
33 Brown CC, Gudjonson H, Pritykin Y, *et al*. Transcriptional basis of mouse and human dendritic cell heterogeneity. *Cell* 2019;179:846–63.
34 Bourdely P, Anselmi G, Vaivode K, *et al*. Transcriptional and functional analysis of CD1c+ human dendritic cells identifies a CD163+ subset priming CD8+CD103+ T cells. *Immunity* 2020;53:335–52.
35 Dutertre C-A, Becht E, Irac SE, *et al*. Single-cell analysis of human mononuclear phagocytes reveals subset-defining markers and identifies circulating inflammatory dendritic cells. *Immunity* 2019;51:573–89.
36 Villani A-C, Satija R, Reynolds G, *et al*. Single-cell RNA-seq reveals new types of human blood dendritic cells, monocytes, and progenitors. *Science* 2017;356:1. doi:10.1126/science.aah4573
37 Aibar S, González-Blas CB, Moerman T, *et al*. SCENIC: single-cell regulatory network inference and clustering. *Nat Methods* 2017;14:1083–6.
38 Liberzon A, Subramanian A, Pinchback R. MSigDB 3.0. *Bioinformatics* 2011;27:1739–40.
39 Patro R, Duggal G, Love MI, *et al*. Salmon provides fast and bias-aware quantification of transcript expression. *Nat Methods* 2017;14:417–9.
40 Love MI, Huber W, Anders S. Moderated estimation of fold change and dispersion for RNA-seq data with DESeq2. *Genome Biol* 2014;15:550.
41 Saito H, Okita K, Chang AE, *et al*. Adoptive transfer of CD8+ T cells generated from induced pluripotent stem cells triggers regressions of large tumors along with immunological memory. *Cancer Res* 2016;76:3473–83.
42 Lee J, Breton G, Oliveira TYK, *et al*. Restricted dendritic cell and monocyte progenitors in human cord blood and bone marrow. *J Exp Med* 2015;212:385–99.
43 Breton G, Lee J, Zhou YJ, *et al*. Circulating precursors of human CD1c+ and CD141+ dendritic cells. *J Exp Med* 2015;212:401–13.
44 See P, Dutertre C-A, Chen J, *et al*. Mapping the human DC lineage through the integration of high-dimensional techniques. *Science* 2017;356 doi:10.1126/science.aag3009
45 Cytlak U, Resteu A, Pagan S, *et al*. Differential IRF8 transcription factor requirement defines two pathways of dendritic cell development in humans. *Immunity* 2020;53:353–70.
46 Villar J, Segura E. Decoding the heterogeneity of human dendritic cell subsets. *Trends Immunol* 2020;41:1062–71.
47 De Smedt M, Taghon T, Van de Walle I, *et al*. Notch signaling induces cytoplasmic CD3 epsilon expression in human differentiating NK cells. *Blood* 2007;110:2696–703.
48 Yin X, Yu H, Jin X, *et al*. Human blood CD1c+ dendritic cells encompass CD5high and CD5low subsets that differ significantly in phenotype, gene expression, and functions. *J Immunol* 2017;198:1553–64.
49 Hao Y, Hao S, Andersen-Nissen E, *et al*. Integrated analysis of multimodal single-cell data. *Cell* 2021;184:3573–87.
50 Satoh T, Toledo MAS, Boehnke J, *et al*. Human DC3 antigen presenting dendritic cells from induced pluripotent stem cells. *Front Cell Dev Biol* 2021;9:667304.
51 Sontag S, Förster M, Qin J, *et al*. Modelling IRF8 deficient human hematopoiesis and dendritic cell development with engineered iPS cells. *Stem Cells* 2017;35:898–908.
52 Jongbloed SL, Kassianos AJ, McDonald KJ, *et al*. Human CD141+ (BDCA-3)+ dendritic cells (DCs) represent a unique myeloid DC subset that cross-presents necrotic cell antigens. *J Exp Med* 2010;207:1247–60.
53 Crozat K, Guiton R, Contreras V, *et al*. The XC chemokine receptor 1 is a conserved selective marker of mammalian cells homologous to mouse CD8α+ dendritic cells. *J Exp Med* 2010;207:1283–92.
54 Bachem A, Güttler S, Hartung E, *et al*. Superior antigen cross-presentation and XCR1 expression define human CD11c+CD141+ cells as homologues of mouse CD8+ dendritic cells. *J Exp Med* 2010;207:1273–81.
55 Oba T, Long MD, Keler T, *et al*. Overcoming primary and acquired resistance to anti-PD-L1 therapy by induction and activation of tumor-residing cDC1s. *Nat Commun* 2020;11:5415.
56 Oba T, Makino K, Kajihara R, *et al*. In situ delivery of iPSC-derived dendritic cells with local radiotherapy generates systemic antitumor immunity and potentiates PD-L1 blockade in preclinical poorly immunogenic tumor models. *J Immunother Cancer* 2021;9:e002432.
57 Hammerich L, Marron TU, Upadhyay R, *et al*. Systemic clinical tumor regressions and potentiation of PD1 blockade with in situ vaccination. *Nat Med* 2019;25:814–24.
58 Hegde S, Krisnawan VE, Herzog BH, *et al*. Dendritic cell paucity leads to dysfunctional immune surveillance in pancreatic cancer. *Cancer Cell* 2020;37:289–307.
59 Patel A, Oba T, Kajihara R, *et al*. Multimodal intralesional therapy for reshaping the myeloid compartment of tumors resistant to anti-PD-L1 therapy via IRF8 expression. *J Immunol* 2021;207:1298–309.
60 Barnawi R, Al-Khaldi S, Majed Sleiman G, *et al*. Fascin is critical for the maintenance of breast cancer stem cell pool predominantly via the activation of the Notch self-renewal pathway. *Stem Cells* 2016;34:2799–813.

Suppl. Fig. 1

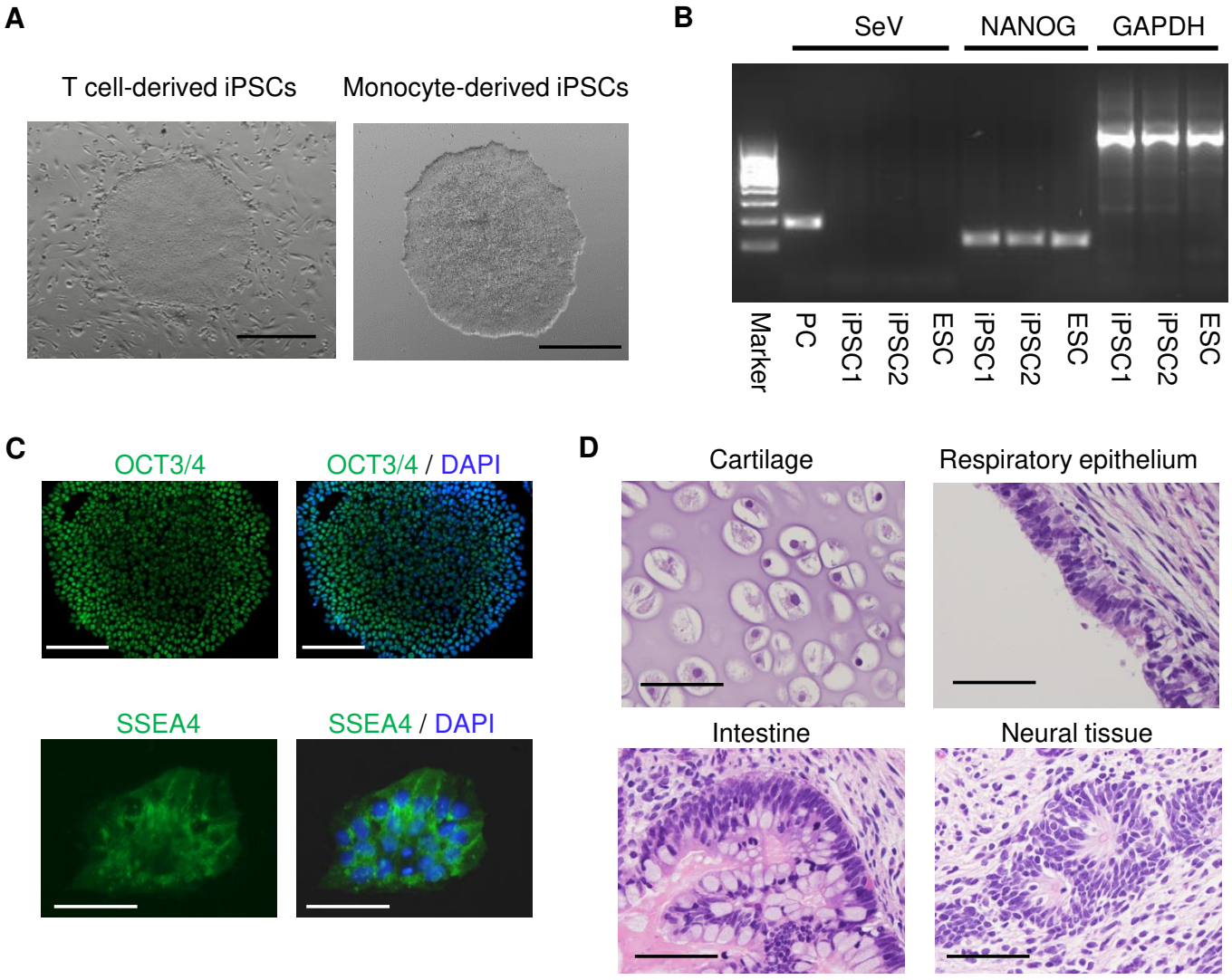

Supplementary Figure 1 Generation of human iPSCs from peripheral blood mononuclear cells.

A, Morphology of human iPSCs. Scale bar, 500 µm.

B, RT-PCR analysis for the human embryonic stem cell (ESC) marker gene, *NANOG* and Sendai virus (SeV) vector in human T-cell derived iPSC #1, 2 and ESCs. PC: positive control

C, ES cell markers, OCT3/4 and SSEA4 in human iPSCs. Nuclei were counterstained with DAPI. Scale bars, 500 µm.

D, Hematoxylin and eosin–stained representative teratomas derived from human iPSCs. Scale bars, 50 µm. Data shown are representative of two independent experiments.

Suppl. Fig. 2

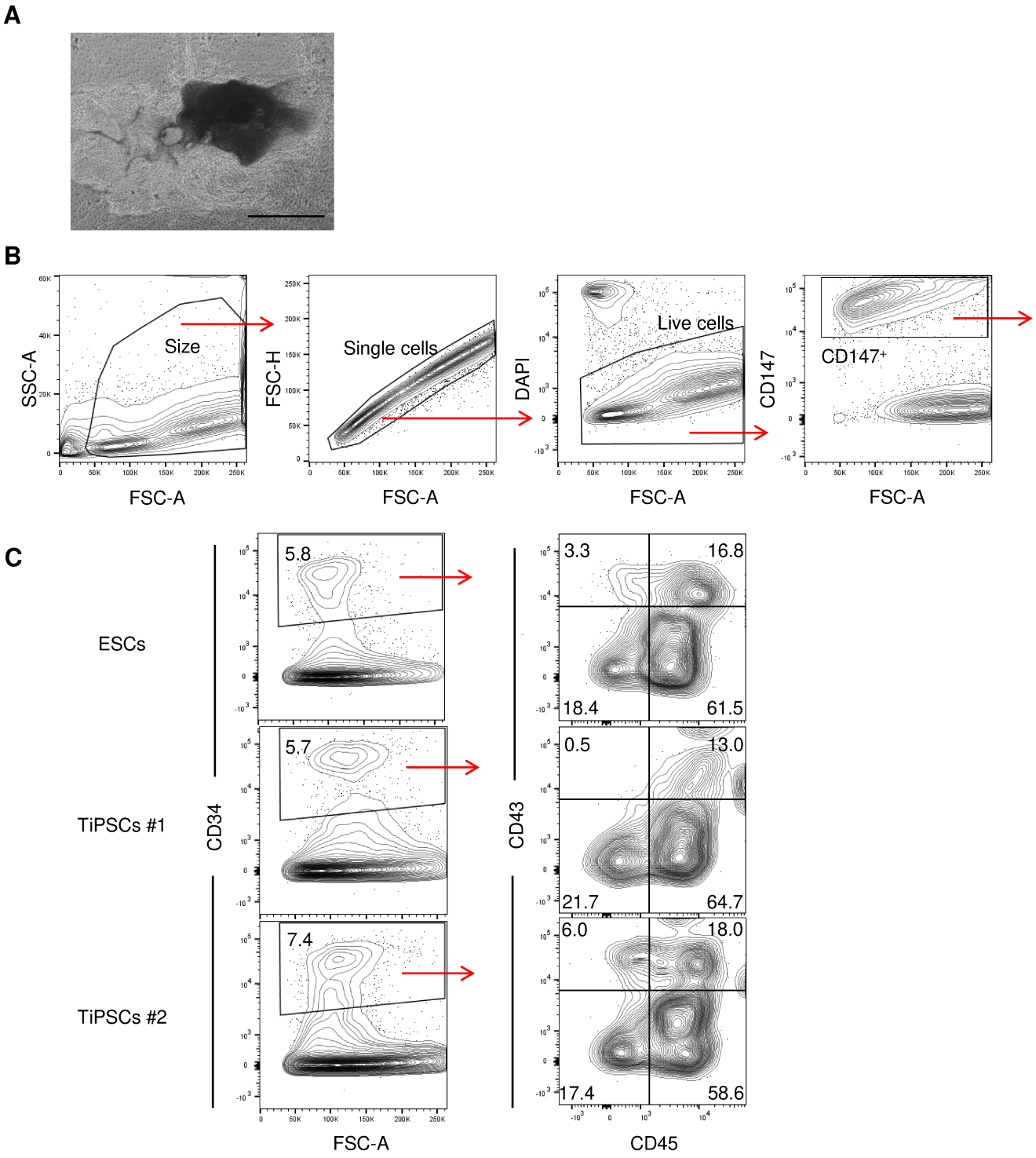

Supplementary Figure 2 Generation of hematopoietic progenitor cells from human iPSCs.

A, Morphology of human iPSC-derived cells differentiated on OP9 feeder cells (day 13). Scale bar, 500 µm.

B, Gating strategy of identifying human ESC- and iPSC-derived CD34+ hematopoietic progenitor cells. CD147 is a pan-human marker.

C, Representative flow cytometric plots showing marker expression of human ESC- and iPSC-derived cells differentiated on OP9 feeder cells. T-iPSC, T cell-derived iPSC. Number denotes percent positive cells for each marker. Data shown are representative of two independent experiments.

Suppl. Fig. 3

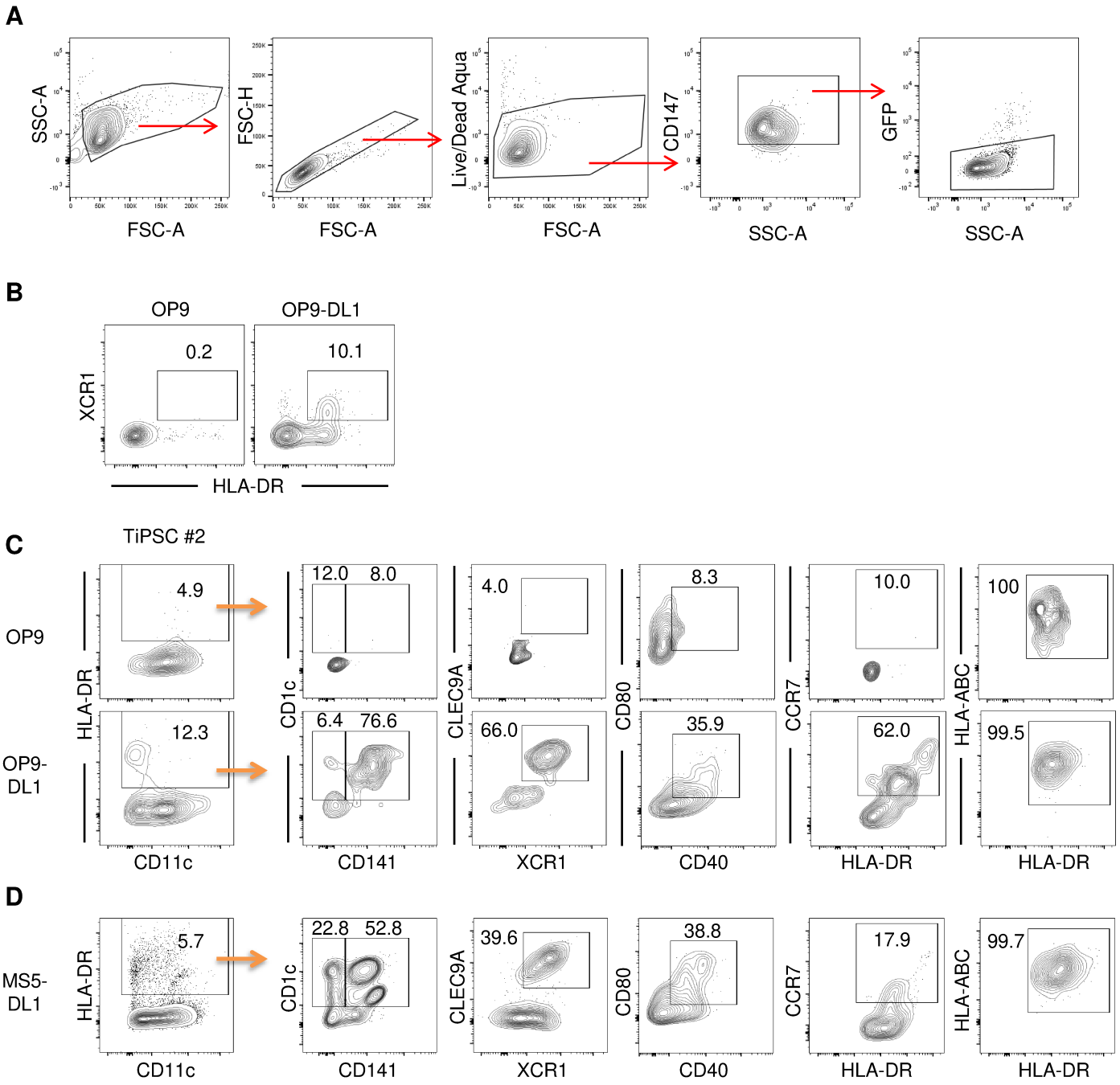

Supplementary Figure 3 Generation of cDC1-like cells from human iPSCs. Related to Fig. 1.

A, Gating strategy of identifying human iPSC-derived CD147^{+} GFP^{-} cells differentiated on OP9 or OP9-DL1 feeder cells. GFP^{-} cells were gated because OP9-DL1 cells express GFP.

B-D, Representative flow cytometric plots showing marker expression of human ESC- (B) and iPSC- (C, D) derived cells differentiated on OP9, OP9-DL1 (B, C), and MS5-DL1 (D) feeder cells. Gated on live CD16^{-} CD88^{-} (B) and on live CD147^{+}GFP^{-} (C, D) cells. T-iPSC, T cell-derived iPSC. Number denotes percent positive cells for each marker. Data shown are representative of two independent experiments.

Suppl. Fig. 4

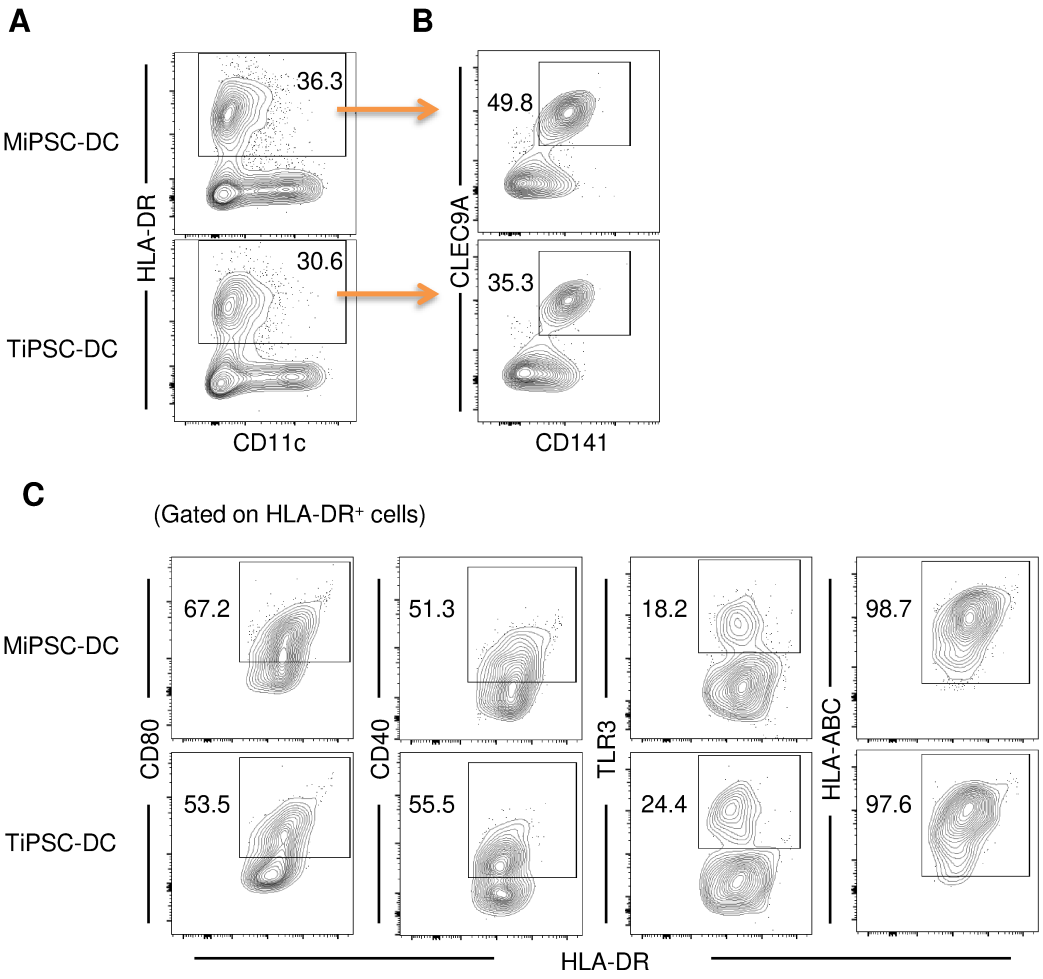

Supplementary Figure 4 Generation of cDC1-like cells from human iPSCs. Related to Figure 1.

A-C, Representative flow cytometric plots showing marker expression of human iPSC-derived cells differentiated on OP9-DL1 feeder cells. M-iPSC: monocyte-derived iPSC, T-iPSC: T cell-derived iPSC Number denotes percent positive cells for each marker. Data shown are representative of two independent experiments.

Suppl. Fig. 5

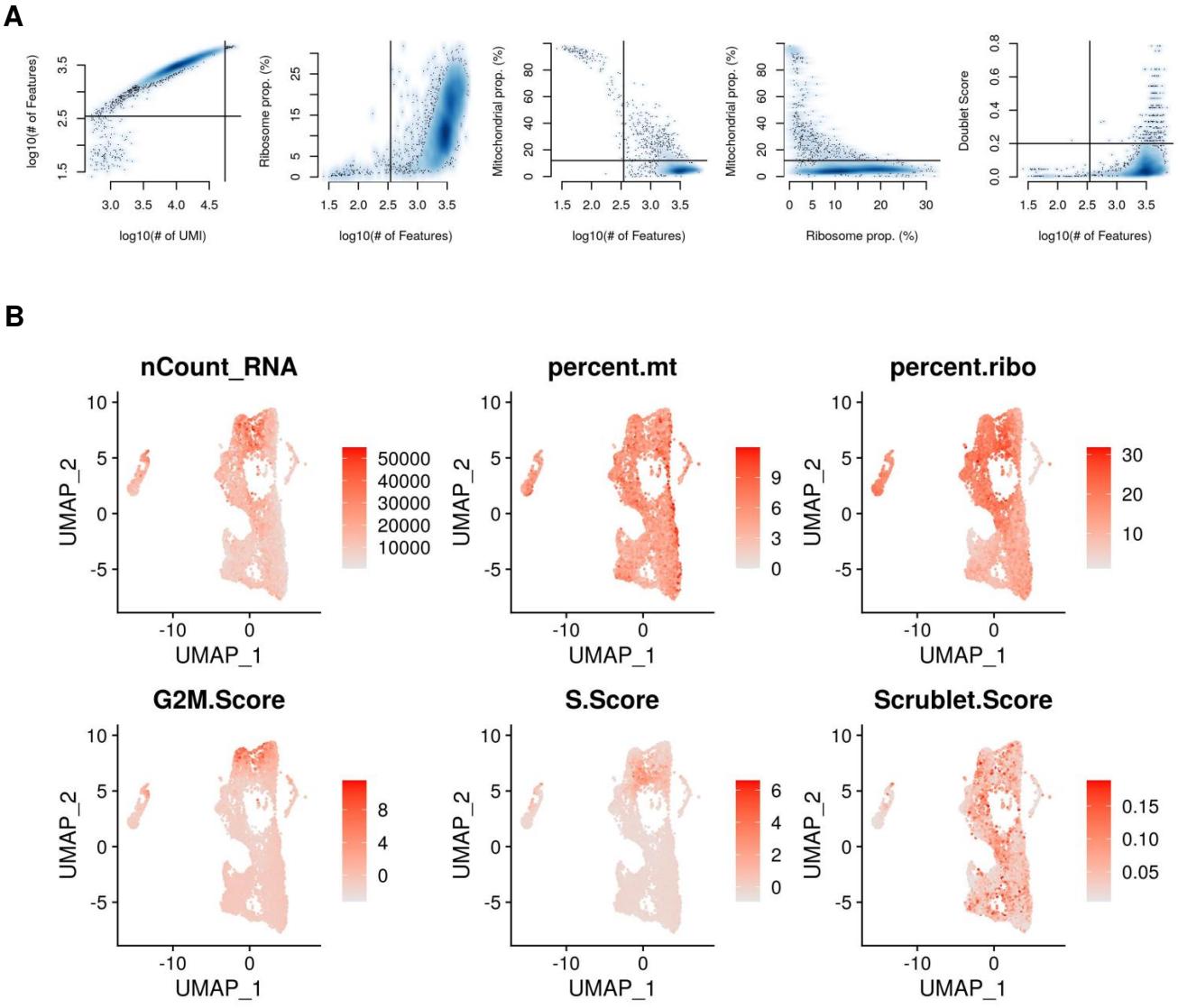

Supplementary Figure 5 Single-cell RNA sequencing (scRNAseq) quality assessment.

A, Scatterplots depicting total features, counts, doublet scores, mitochondrial content and ribosomal content across all cells prior to filtering . Filtering thresholds applied are shown.

B, UMAP representations of all-post filtered, normalized cells showing cellular distributions of total unique counts, mitochondrial scores, ribosomal scores, G2M/S phase scores and doublet scores.

Suppl. Fig. 6

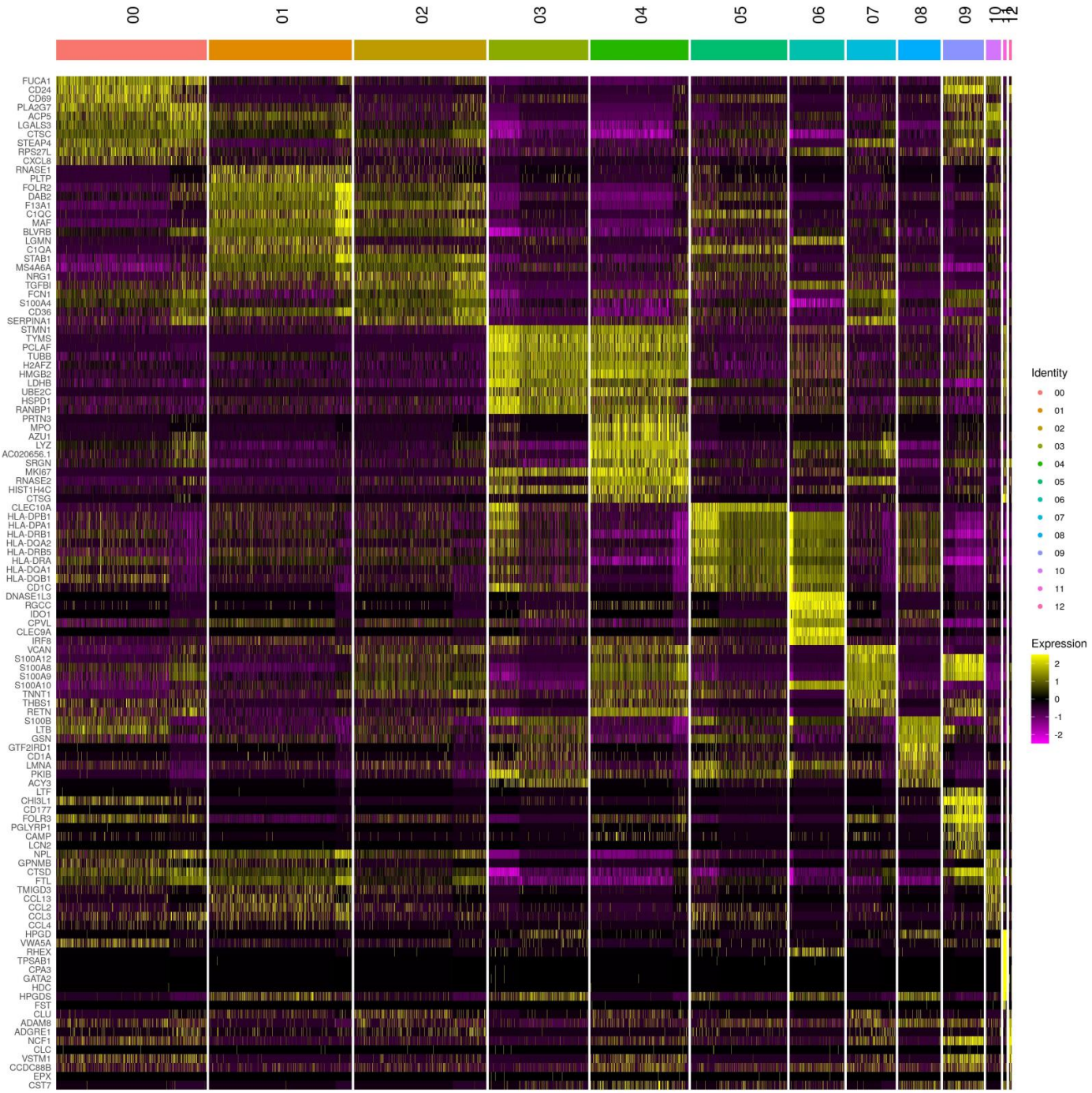

Supplementary Figure 6 Analysis of human iPSC-derived HLA-DR$^+$ cells differentiated on OP9 and OP9-DL1 cells by scRNAseq.

Heatmap of all 8,929 cells showing the expression levels of 10 most discriminative genes per cell type (in rows) across all the identified cell populations (in columns). Color-code layout: scale of purple to yellow; from lowest expression to highest expression.

Suppl. Fig. 7

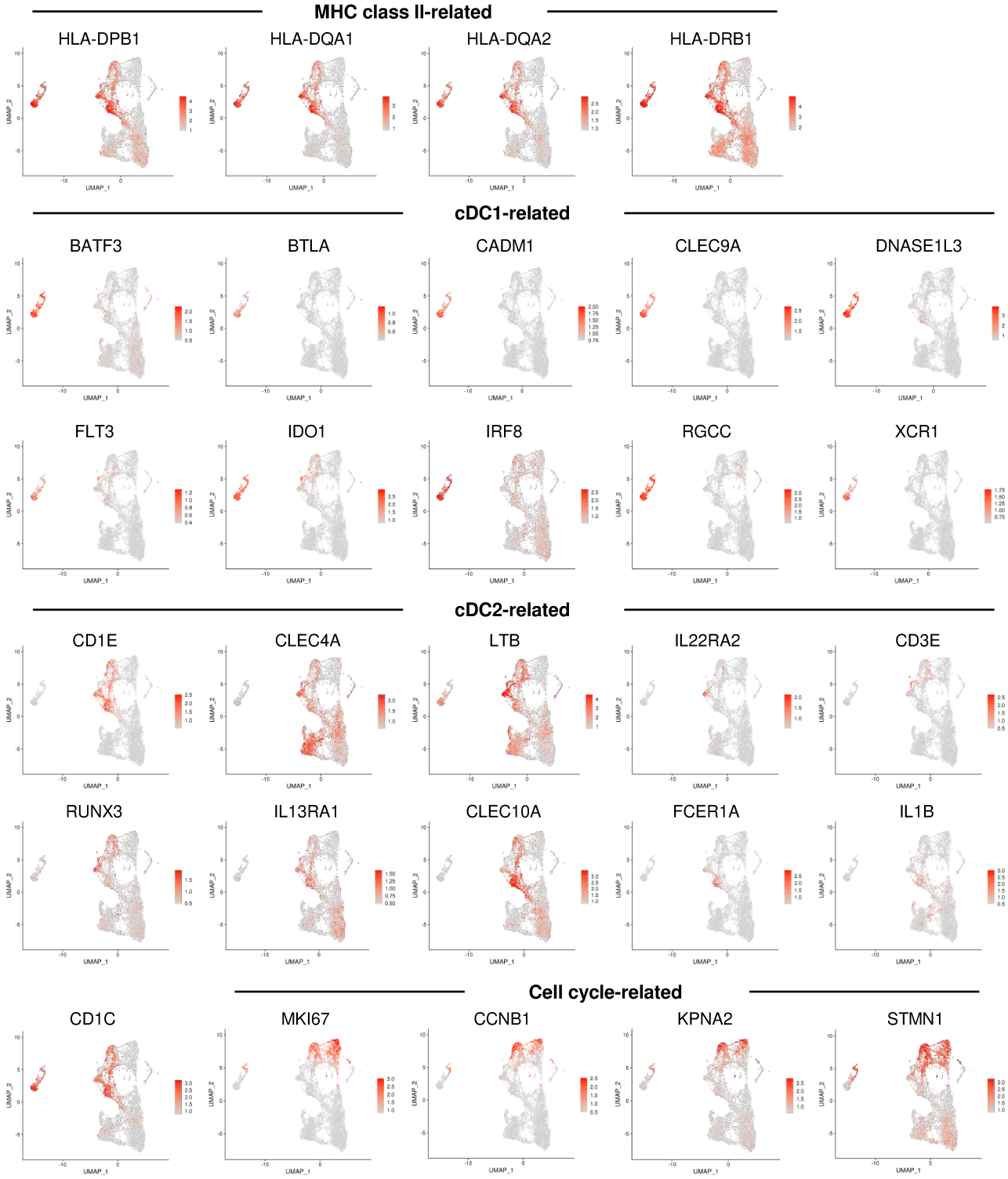

Supplementary Figure 7 Expression plots of indicated genes in human iPSC-derived HLA-DR⁺ clusters.

Expression of indicated genes illustrated in UMAP plots. Expression levels are color-coded: gray, not expressed; red, expressed.

Suppl. Fig. 8

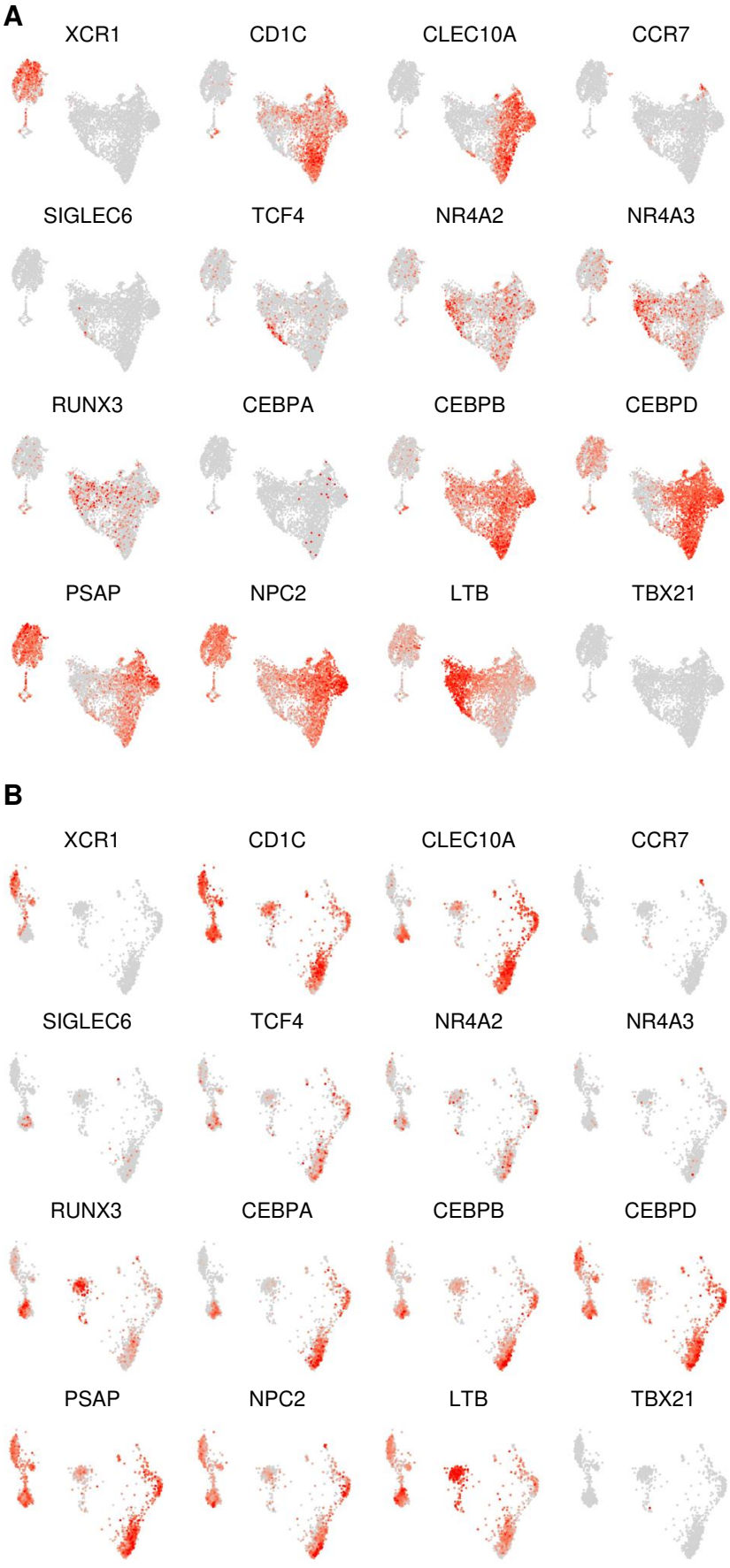

Supplementary Figure 8 Expression plots of indicated genes. Related to Figure 3A, B

A, Expression plots of indicated genes in human splenocytes from Brown et al. (2020).

B, Expression of indicated genes in UMAP generated from projection of clusters 3, 5, 6 and 8 from Fig. 2 of human iPSC-derived HLA-DR$^+$ cells differentiated on OP9 and OP9-DL1 cells onto human splenocyte atlas generated by Brown et al. (2020).

Expression levels are color-coded: gray, not expressed; red, expressed.

Suppl. Fig. 9

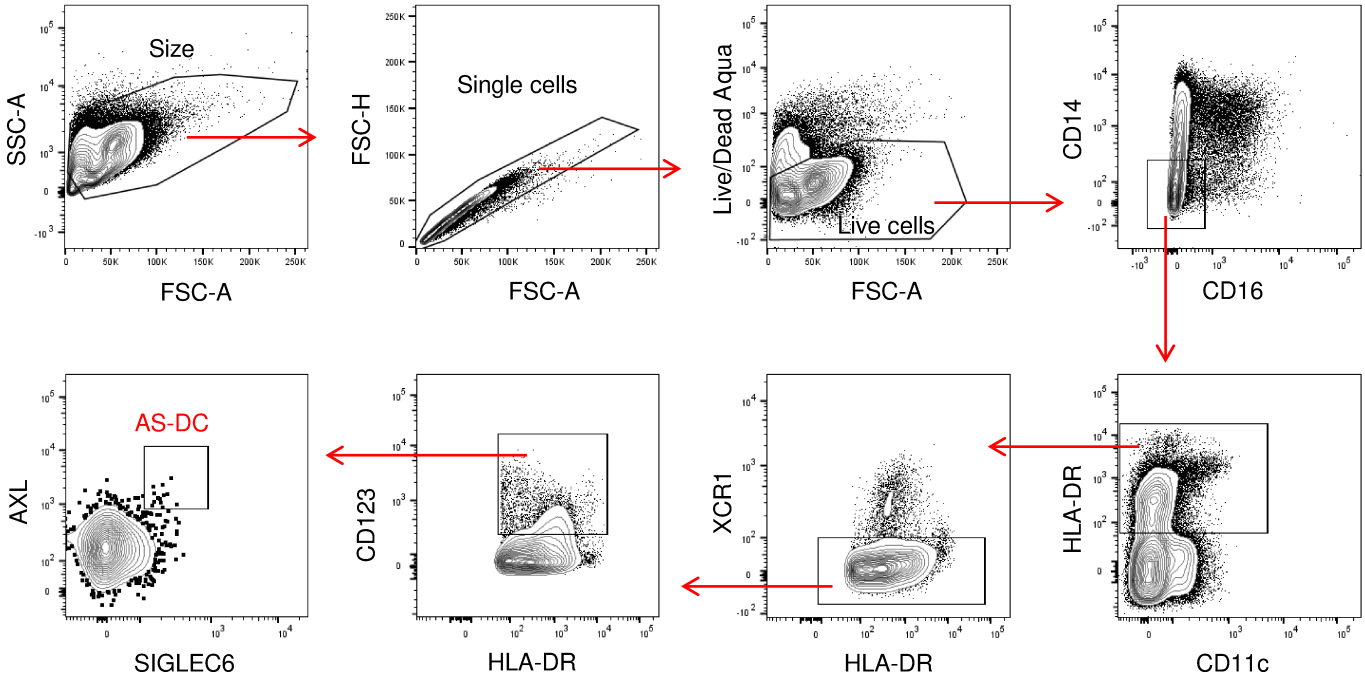

Supplementary Figure 9 Gating strategy of identifying AS-DCs in human iPSC-derived HLA-DR⁺ cells differentiated on OP9 or OP9-DL1 feeder cells. Related to Figure 3D.

Suppl. Fig. 10

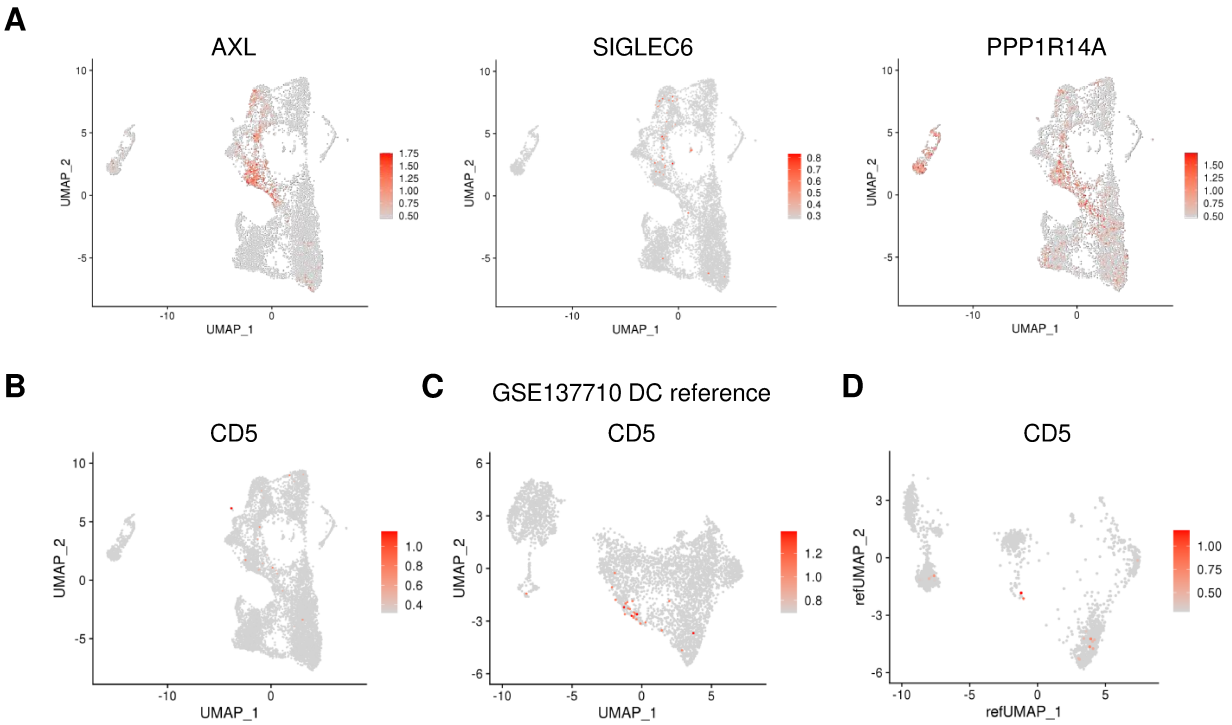

Supplementary Figure 10 Expression plots of indicated genes. Related to Figure 3C, D

A-D, Expression of indicated genes illustrated in UMAP plots. Expression levels are color-coded: gray, not expressed; orange, expressed.

A-D, Expression of AXL, SIGLEC6, PPP1R14A, and CD5 in human iPSC-derived HLA-DR^{+} cells differentiated on OP9 and OP9-DL1 cells.

C, Expression plots of CD5 in human splenocytes from Brown et al. (2020).

D, Expression of CD5 in UMAP plot generated from projection of clusters 3, 5, 6 and 8 from Fig. 2 of human iPSC-derived HLA-DR^{+} cells differentiated on OP9 and OP9-DL1 cells onto human splenocyte atlas generated by Brown et al. (2020).

Suppl. Fig. 11

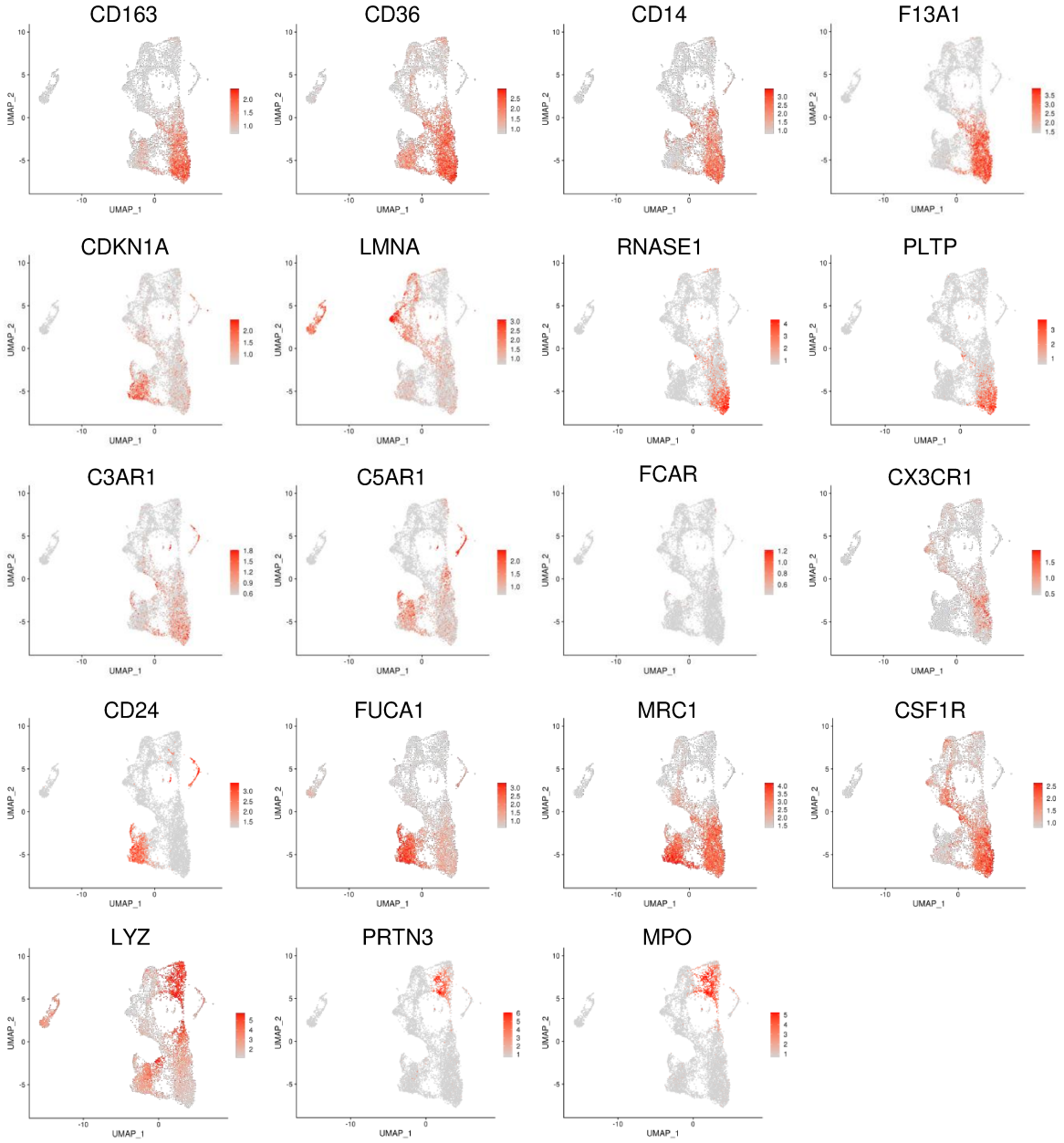

Supplementary Figure 11 Expression plots of indicated genes in human iPSC-derived HLA-DR⁺ clusters.

Expression of indicated genes illustrated in UMAP plots. Expression levels are color-coded: gray, not expressed; orange, expressed.

Suppl. Fig. 12

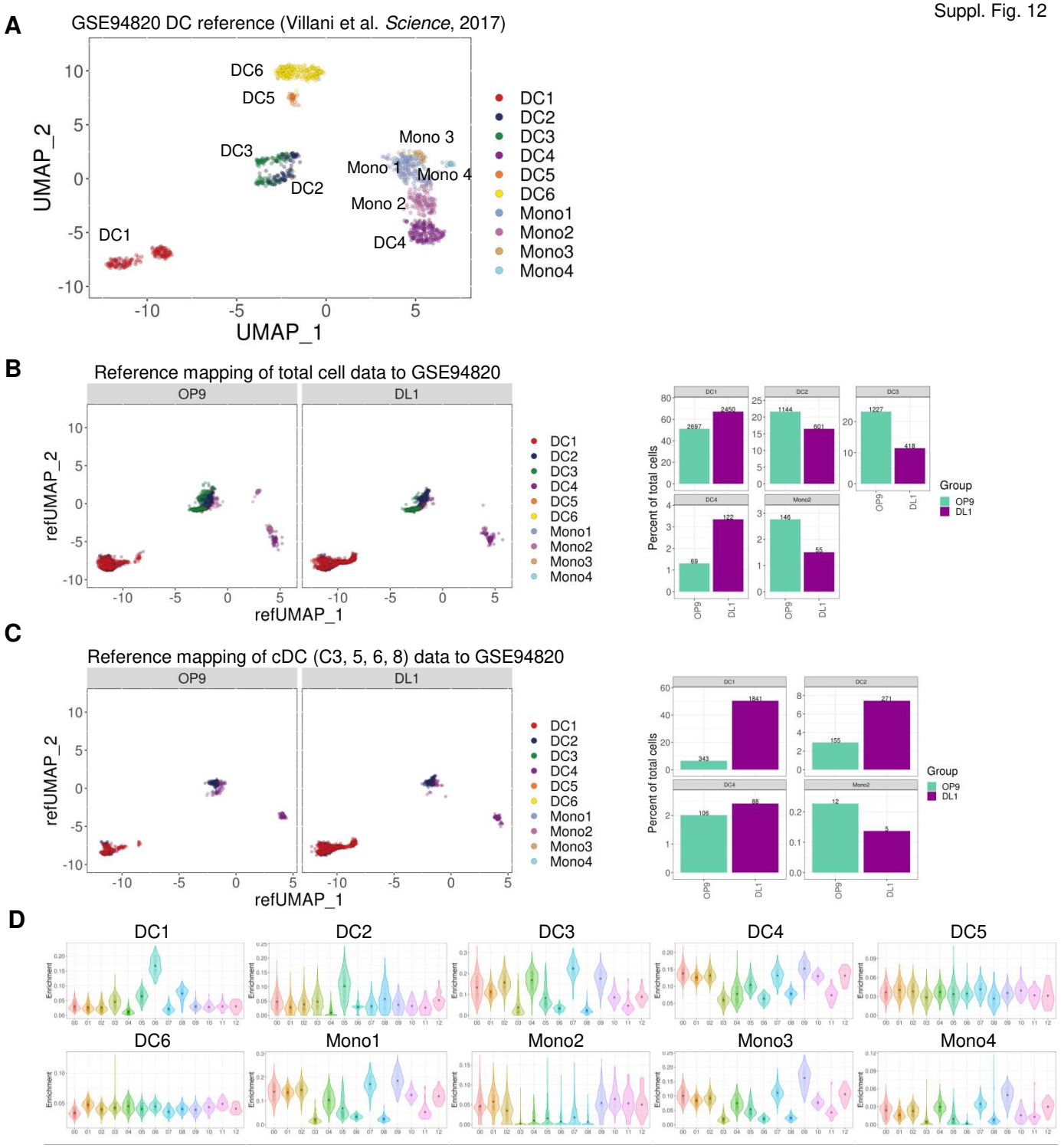

Supplementary Figure 12 Heterogeneity of cDC1⁺ DCs differentiated from human iPSCs. Related to Figure 3E.

A, UMAP plot of Lin(CD3, CD56, CD19)⁻ DC (HLA-DR⁺CD11c⁺CD14⁻)/monocyte (CD14$^{lo/+}$) derived from human PB as described by Villani et al. (2017), colored by cell type.

B, C, UMAP plot of total cells (B) and clusters 3, 5, 6, and 8 (C) from Fig. 2 of human iPSC-derived HLA-DR⁺ cells differentiated on OP9 and OP9-DL1 cells derived from projection onto human peripheral DC/monocyte atlas generated by Villani et al. (2017). Frequency of each cluster is shown. Numbers above each bar graph indicate the total number of cells.

D, Violin plots showing single-cell enrichment scores in each cluster from total cells in Fig. 2 of human iPSC-derived HLA-DR⁺ cells differentiated on OP9 and OP9-DL1 cells using gene sets differentiating each cell type identified in human peripheral DC/monocyte atlas generated by Villani et al. (2017).

Suppl. Fig. 13

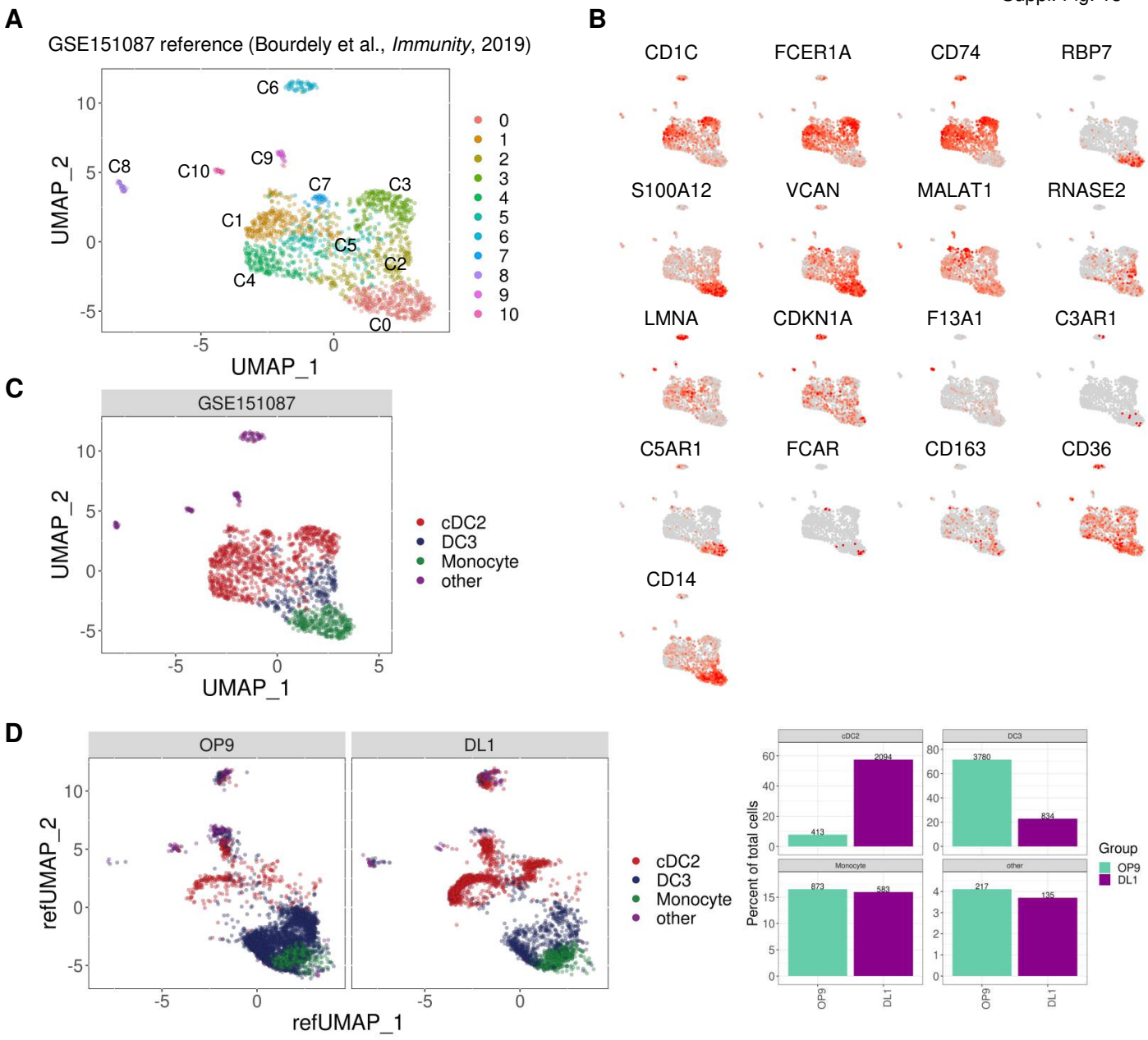

Supplementary Figure 13 Heterogeneity of cDC1⁺ DCs differentiated from human iPSCs. Related to Figure 3F.

A, UMAP plot of human PB CD16⁻CD123⁻CD141⁻CD14$^{+/-}$ CD1c⁺ cells from Bourdely et al. (2019), colored by computationally determined cluster.

B, Expression plots of indicated genes in human PB CD16⁻CD123⁻CD141⁻CD14$^{+/-}$ CD1c⁺ cells from Bourdely et al. (2019).

C, UMAP plot of human PB CD16⁻CD123⁻CD141⁻CD14$^{+/-}$ CD1c⁺ cells from Bourdely et al. (2019), colored by cell type.

D, UMAP plot of total cells from Fig. 2 of human iPSC-derived HLA-DR⁺ cells differentiated on OP9 and OP9-DL1 cells derived from projection onto human PB CD16⁻CD123⁻CD141⁻CD14$^{+/-}$ CD1c⁺ cells from Bourdely et al. (2019). Frequency of each cluster is shown. Numbers in bar graphs indicates cell numbers in each group.

Suppl. Fig. 14

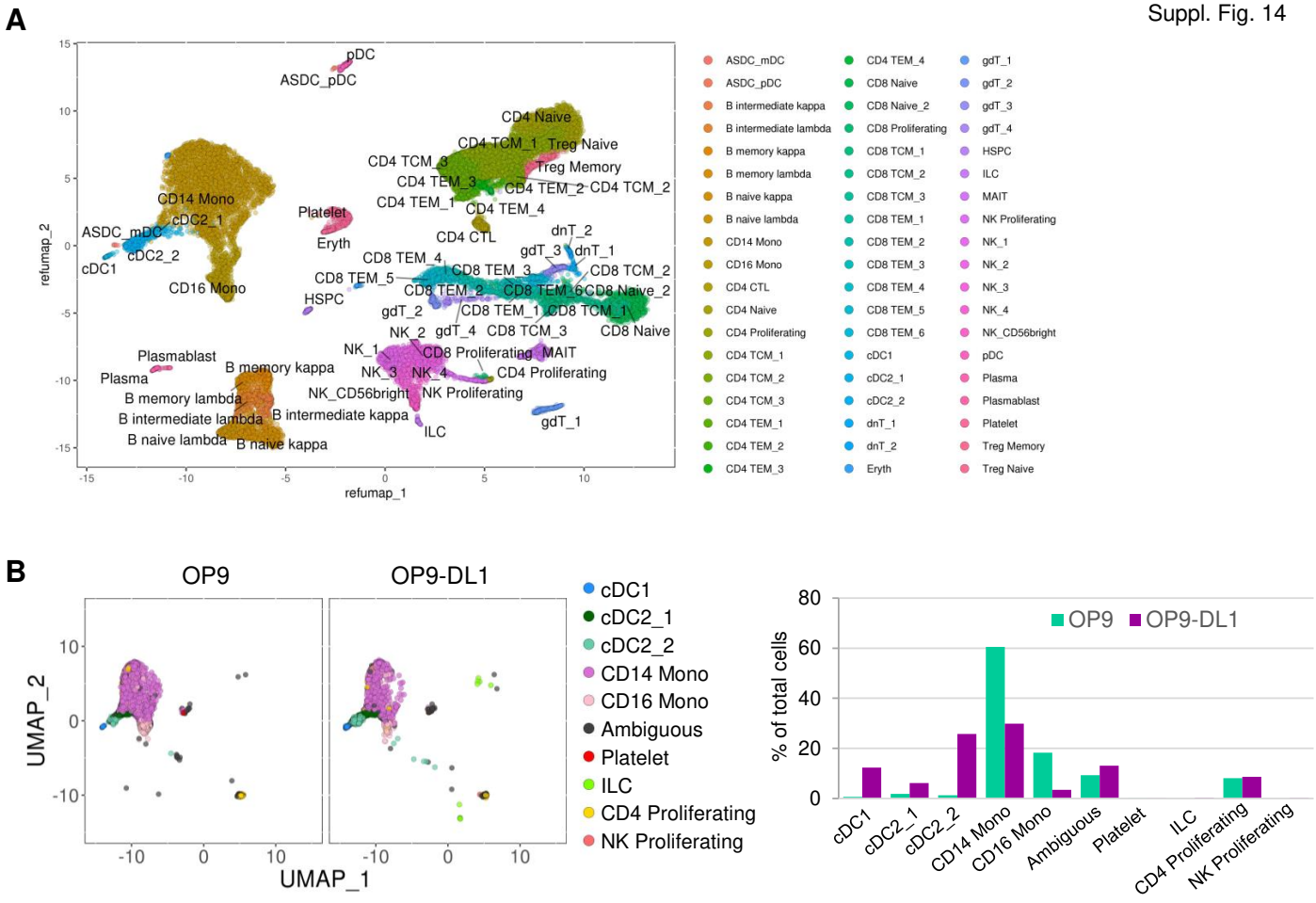

Supplementary Figure 14 Plasmacytoid DCs (pDCs) are not differentiated from human iPSCs on OP9 or OP9-DL1 cells.

A, UMAP plot of human PBMCs from Hao et al. (2021) https://azimuth.hubmapconsortium.org/.

B, UMAP plot of total cells from Fig. 2 of human iPSC-derived HLA-DR$^+$ cells differentiated on OP9 and OP9-DL1 cells derived from projection onto human PBMC atlas available at https://azimuth.hubmapconsortium.org/. Proportions of predicted cell types are shown (right).

C, Proportions of computationally predicted cell types from projection onto human PBMC atlas by cluster are shown.

Suppl. Fig. 15

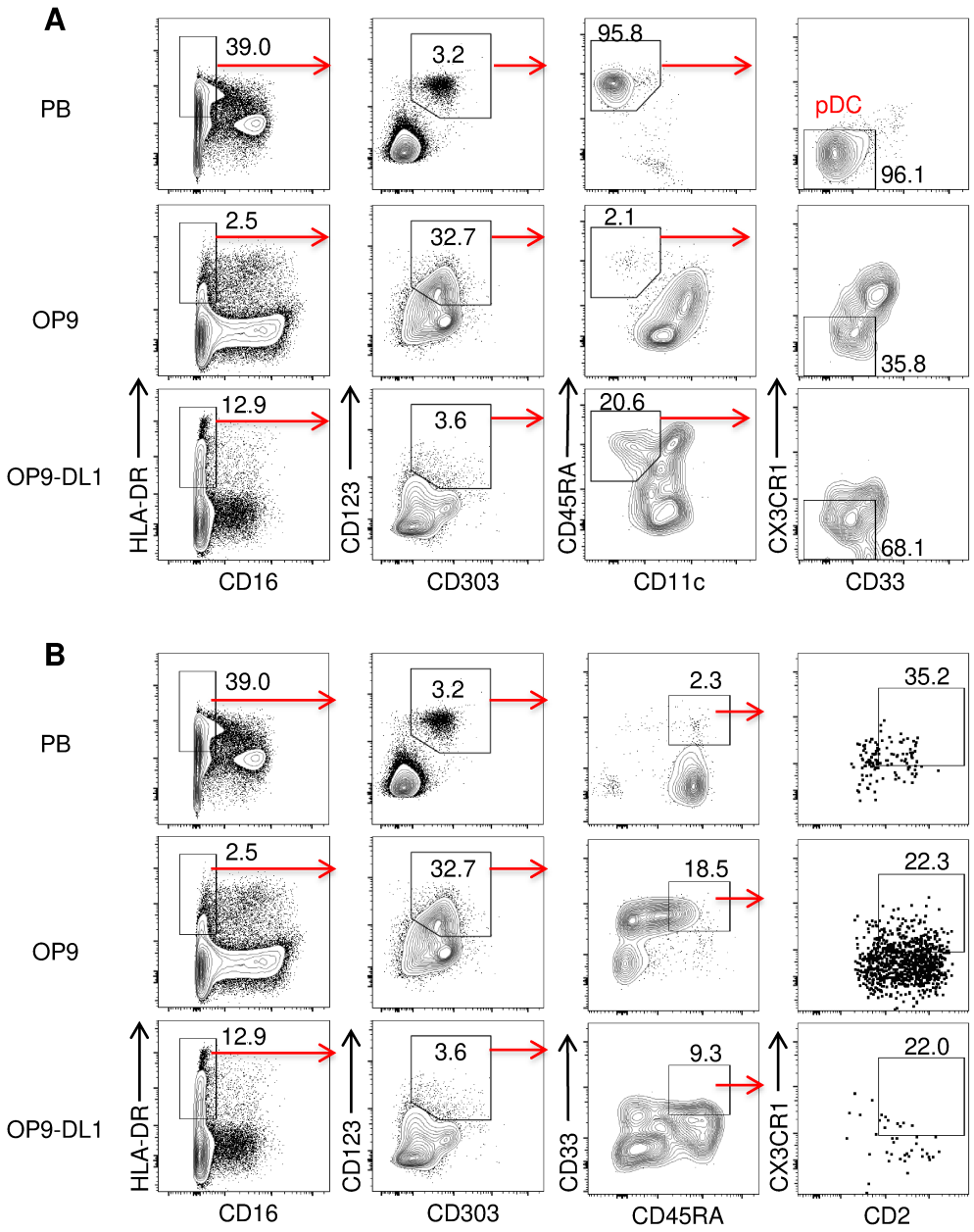

Supplementary Figure 15 human iPSCs did not differentiate to plasmacytoid DCs (pDCs) on OP9 or OP9-DL1 feeder cells.

A, B, Representative flow cytometric plots showing marker expression of peripheral blood (PB) and human iPSC-derived cells differentiated on OP9 or OP9-DL1 feeder cells. Gating strategy is shown in supplementary figure 3A. Number denotes percent positive cells for each gated population. Data shown are representative of two independent experiments.

Suppl. Fig. 16

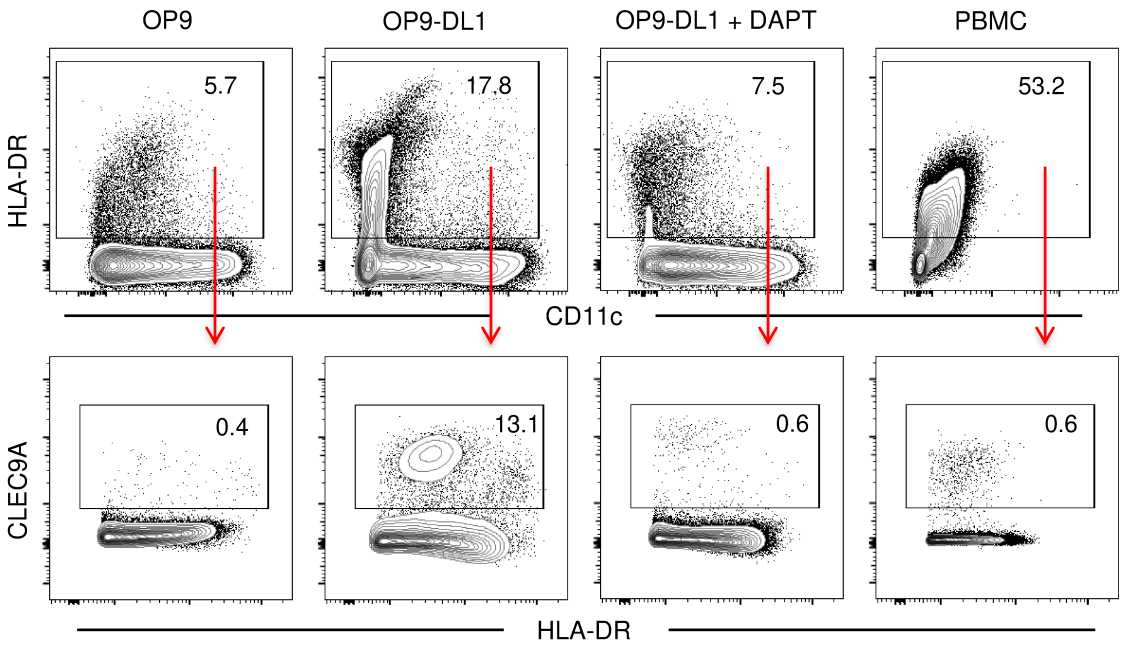

Supplementary Figure 16 Non-redundant requirement of Notch signaling for generation of cDC1s from human iPSCs. Related to Fig. 4A.

Representative flow cytometric plots showing marker expression of human PBMC, or iPSC-derived cells differentiated on OP9, OP9-DL1 cells in the presence or absence of a γ-secretase inhibitor, N-[N-(3,5-difluorophenacetyl)- L-alanyl]-S-phenylglycine t-butyl ester (DAPT). Gated on live single cells. Number denotes percent positive cells for each marker. Data shown are representative of two independent experiments.

Suppl. Fig. 17

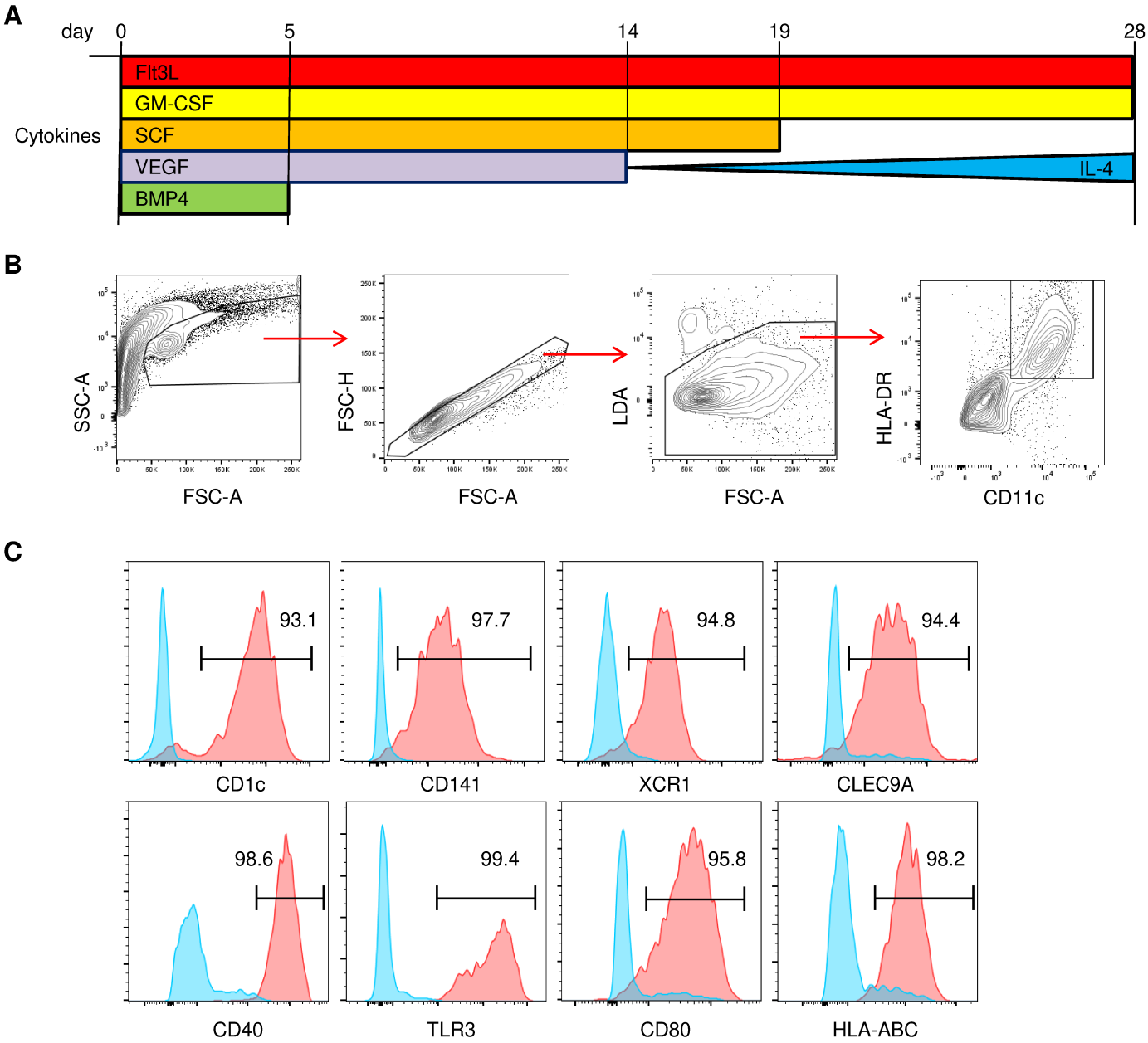

Supplementary Figure 17 Generation of CD141⁺CLEC9A⁺XCR1⁺ DCs from human iPSCs under feeder- and xeno-free conditions.

A, Schedule of growth factors and cytokines.

B, Gating strategy of identifying human iPSC-derived HLA-DR⁺CD11c⁺ DCs differentiated under feeder-free condition (A).

C, Representative histograms showing marker expression of human iPSC-derived HLA-DR⁺CD11c⁺ DCs differentiated under feeder-free condition (A). Number denotes percent positive cells (red) for each marker. Isotype control (blue). Data shown are representative of two independent experiments.

Suppl. Fig. 18

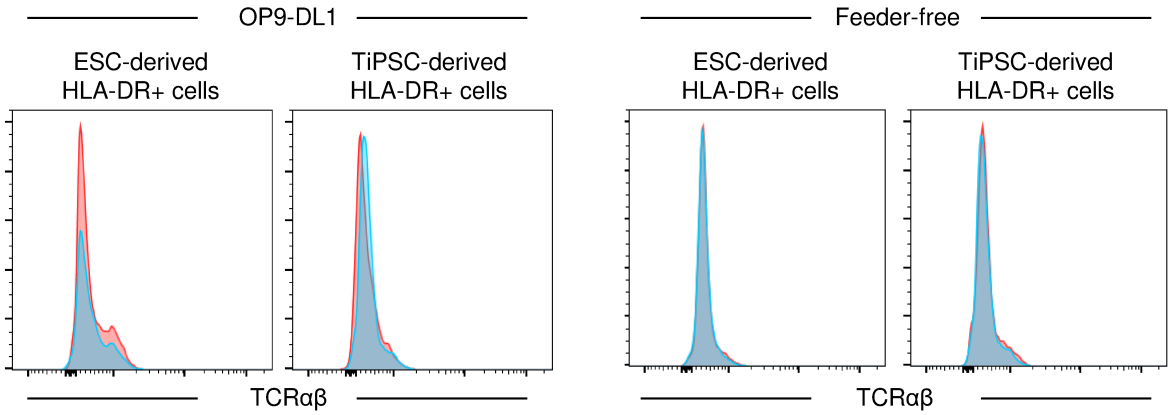

Supplementary Figure 18 ESC- or TiPSC-derived HLA-DR⁺ cells do not express TCRαβ.

Representative histogram showing TCRαβ expression in human ESC- or TiPSC-derived HLA-DR⁺ cells on OP9-DL1 cells (left) or under feeder- and xeno-free condition (right) as described in figure 1A and supplementary figure 17, respectively. TiPSC, T-cell derived iPS cells. Isotype control (blue). Data shown are representative of two independent experiments.

Suppl. Fig. 19

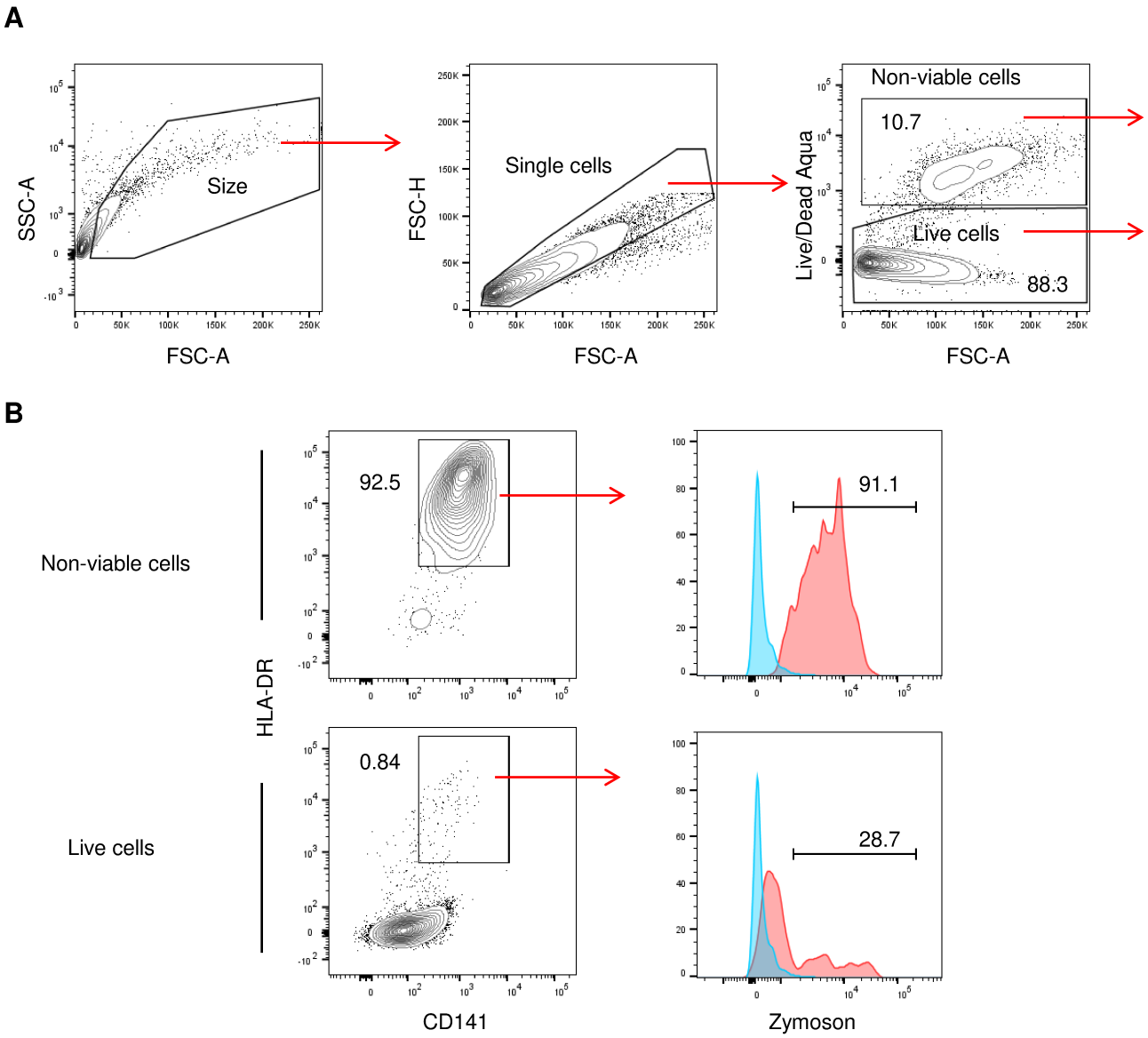

Supplementary Figure 19 The majority of CD141⁺ DCs differentiated from human iPSCs under feeder- and xeno-free conditions are not viable after phagocytosis.

A, Gating strategy of identifying non-viable and live human iPSC-derived CD141⁺ DCs differentiated under feeder- and xeno-free condition.

B, Representative histogram showing zymosan expression in non-viable and live human iPSC-derived CD141⁺ DCs. Number denotes percent positive cells (red) for each marker. No zymosan (blue).

Data shown are representative of two independent experiments.

Suppl. Fig. 20

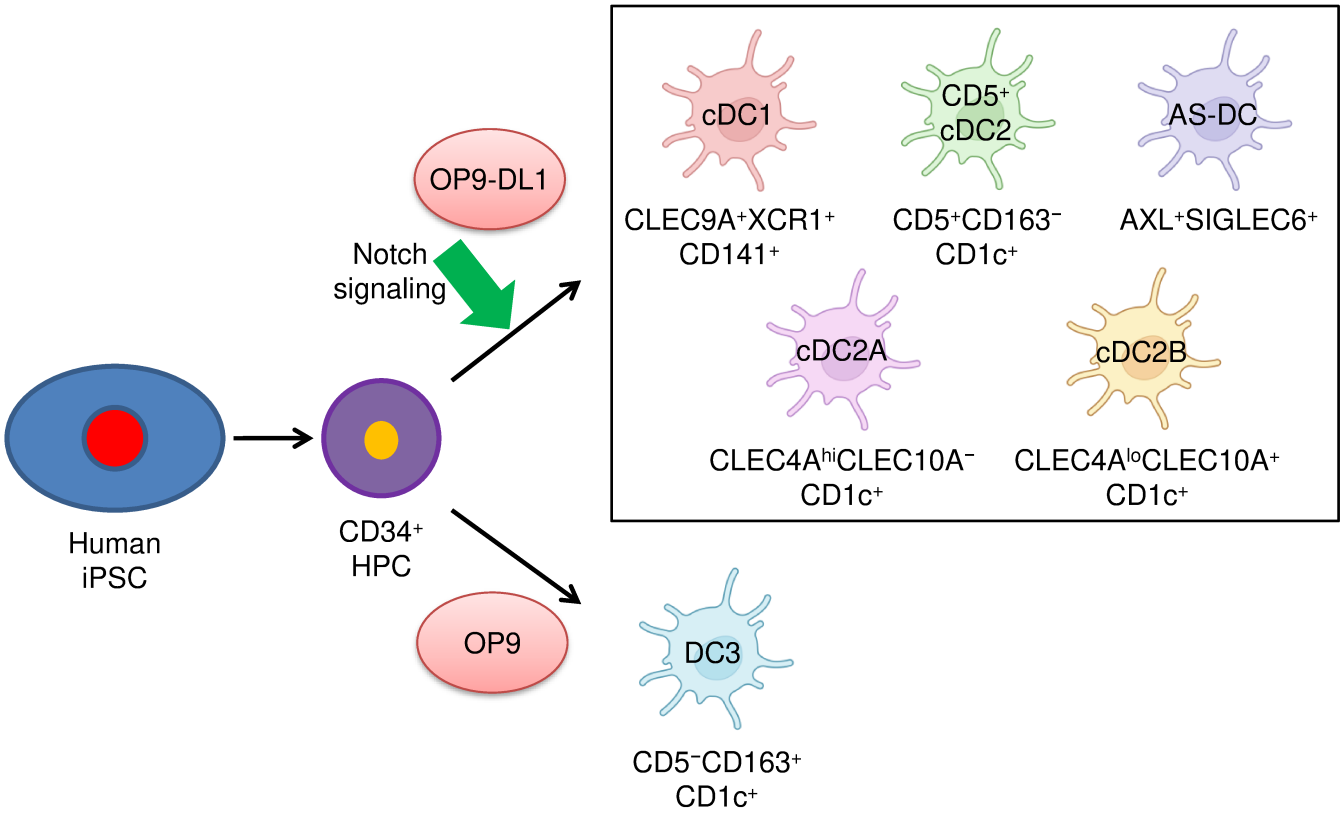

Supplementary Figure 20 Schematic representation of cDC subsets differentiated from human iPSCs

Supplementary Table S1 The sequences of primer sets. (related to Supplementary Fig. 1)

Genes	Sequences (Forward: F, Reverse: R)
SeV	F: GGATCACTAGGTGATATCGAGC
	R: ACCAGACAAGAGTTTAAGAGATATGTATC
NANOG	F: TCCTCCTCTTCCTCTATACTAAC
	R: CCCACAAATCACAGGCATAG
GAPDH	F: TGAAGGTCGGAGTCAACGGATTTGGT
	R: CATGTGGGCCATGAGGTCCACCAC

Supplementary Table S2. List of antibodies

Antibodies	Clones	Vendors
Rat IgG2a, κ Isotype Ctrl	RTK2758	BioLegend
Mouse IgG1, κ Isotype Ctrl	MOPC-21	BioLegend
Mouse IgG2a, κ Isotype Ctrl	MOPC-173	BioLegend
anti-HLA-DR	L243	BD Biosciences
anti-HLA-ABC	G46-2.6	BD Biosciences
anti-CD123	6H6	BioLegend
anti-CD11c	B-ly6	BD Biosciences
anti-CD1c	L161	BioLegend
anti-CD141	M80	BioLegend
anti-CLEC9A	8F9	BioLegend
anti-XCR1	S15046E	BioLegend
anti-CD80	MAB104	Beckman Coulter
anti-CD40	B8.2C12	BioLegend
anti-CD86	2331	BD Biosciences
anti-CCR7	150503	BD Biosciences
anti-CD14	MφP9	BD Biosciences
anti-CD62L	DREG-56	BD Biosciences
anti-CD25	M-A251	BioLegend
anti-CD3	UCHT1	ThermoFisher Scientific
anti-CD4	RPA-T4	BD Biosciences
anti-CD8	SK1	BD Biosciences
anti-CD27	O323	ThermoFisher Scientific
anti-CD147	HIM6	BioLegend
anti-CD34	581	BD Biosciences
anti-CD43	1G10	BD Biosciences
anti-CD45	HI30	BD Biosciences
anti-toll-like receptor 3 (TLR3)	TLR3.7	ThermoFisher Scientific
anti-CD16	3G8	BD Biosciences
anti-CD163	GHI/61	BioLegend
anti-CD303	201A	BioLegend
anti-CX3CR1	2A9-1	BioLegend
anti-CD33	P67.6	BioLegend
anti-CD2	RPA-2.10	BioLegend
anti-CD5	UCHT-2	BioLegend
anti-CLEC10A	H037G3	BioLegend
anti-AXL	108724	R&D Systems
anti-SIGLEC6	767329	R&D Systems
anti-CD45RA	HI100	BioLegend
anti-IL-12p40/70	C8.6	BD Biosciences
anti-TNFα	MAb11	BD Biosciences
anti-IFNα	LT27:295	Miltenyi Biotec
anti-CLEC4A	9E8	BioLegend
anti-CD88	S5/1	BioLegend
anti-IFN-λ1	247801	R&D Systems
anti-TCRα/β	IP26	BioLegend

Supplementary Table S3. Metrics of pre-filtering samples.

(related to Supplementary Fig. 5)

Estimated.Number.of.Cells	5,753	4,158
Mean.Reads.per.Cell	28,290	31,515
Median.Genes.per.Cell	3,018	3,311
Number.of.Reads	162,757,202	131,042,876
Valid.Barcodes	97.50%	97.40%
Sequencing.Saturation	35.70%	31.20%
Q30.Bases.in.Barcode	96.50%	96.50%
Q30.Bases.in.RNA.Read	94.70%	94.40%
Q30.Bases.in.Sample.Index	90.40%	94.20%
Q30.Bases.in.UMI	95.90%	95.80%
Reads.Mapped.to.Genome	97.60%	97.60%
Reads.Mapped.Confidently.to.Genome	95.20%	95.20%
Reads.Mapped.Confidently.to.Intergenic.Regions	3.50%	3.70%
Reads.Mapped.Confidently.to.Intronic.Regions	17.00%	17.20%
Reads.Mapped.Confidently.to.Exonic.Regions	74.70%	74.30%
Reads.Mapped.Confidently.to.Transcriptome	70.40%	70.00%
Reads.Mapped.Antisense.to.Gene	1.30%	1.30%
Fraction.Reads.in.Cells	96.60%	93.60%
Total.Genes.Detected	20,142	20,090
Median.UMI.Counts.per.Cell	9,952	12,758

Supplementary Table S4. Monocyte and cDC1 marker genes described by Balan et al., (related to Fig. 2E)

Monocyte genes	cDC1 genes	
CEBPB	DNASE1L3	CAMK2D
LYZ	GCSAM	XCR1
MNDA	IDO1	RAB7B
S100A6	CNE-3	C1ORF54
CSTA	CADM1	ID2
FCN1	CLEC9A	CPNE3
CD14	BATF3	CLEC7A
S100A12	ZNF366	CXCL16
S100A8	DPP4	CCND1
S100A9	CLNK	SNX22
VCAN	CD83	SLAMF7
	THBD	SLAMF8
	SEPT3	LY75